ARTICLE

TGF-β regulates the stem-like state of PD-1+ TCF-1+ virus-specific CD8 T cells during chronic infection

Yinghong Hu[1], William H. Hudson[1], Haydn T. Kissick[1,2,3], Christopher B. Medina[1], Antonio P. Baptista[4,5,8], Chaoyu Ma[6], Wei Liao[6,7], Ronald N. Germain[8], Shannon J. Turley[9], Nu Zhang[6], and Rafi Ahmed[1]

Recent studies have defined a novel population of PD-1+ TCF-1+ stem-like CD8 T cells in chronic infections and cancer. These quiescent cells reside in lymphoid tissues, are critical for maintaining the CD8 T cell response under conditions of persistent antigen, and provide the proliferative burst after PD-1 blockade. Here we examined the role of TGF-β in regulating the differentiation of virus-specific CD8 T cells during chronic LCMV infection of mice. We found that TGF-β signaling was not essential for the generation of the stem-like CD8 T cells but was critical for maintaining the stem-like state and quiescence of these cells. TGF-β regulated the unique transcriptional program of the stem-like subset, including upregulation of inhibitory receptors specifically expressed on these cells. TGF-β also promoted the terminal differentiation of exhausted CD8 T cells by suppressing the effector-associated program. Together, the absence of TGF-β signaling resulted in significantly increased accumulation of effector-like CD8 T cells. These findings have implications for immunotherapies in general and especially for T cell therapy against chronic infections and cancer.

Introduction

CD8 T cell exhaustion, driven by persistent antigen, occurs during chronic infections and cancer (Gallimore et al., 1998; Hashimoto et al., 2018; McLane et al., 2019; Zajac et al., 1998). Exhausted CD8 T cells are characterized by sustained upregulation and coexpression of several inhibitory receptors, with programmed cell death 1 (PD-1) playing a critical role in regulating CD8 T cell exhaustion (Barber et al., 2006; Day et al., 2006; Wherry et al., 2007). Antibodies blocking the immune checkpoint PD-1/PD-L1 enhance CD8 T cell response and have been licensed to treat various types of human cancer (Brahmer et al., 2012; Gong et al., 2018; Topalian et al., 2012; Vaddepally et al., 2020).

During chronic infections and cancer, there is a subpopulation of antigen-specific PD-1+ CD8 T cells that show high expression of the transcription factor T cell factor 1 (TCF-1) and the chemokine receptor CXC motif chemokine receptor 5 (CXCR5), and possess stem cell–like properties (Brummelman et al., 2018; He et al., 2016; Im et al., 2016; Utzschneider et al., 2016). These antigen-specific stem-like CD8 T cells undergo slow self-renewal and also serve as the resource for further CD8 T cell differentiation during chronic antigen exposure (Im et al., 2016; Im et al., 2020). These PD-1+ stem-like CD8 T cells found during chronic infection possess a transcriptional and epigenetic signature that is distinct from effector and memory CD8 cells generated during acute infections (Hashimoto et al., 2018; Jadhav et al., 2019; McLane et al., 2019). One key feature of this subset is that they are predominantly localized in the T cell zones of lymphoid tissues in chronically infected mice, away from the major sites of lymphocytic choriomeningitis virus (LCMV) infection, which may protect them from overstimulation by persistent antigen. Parabiosis study showed that these cells were resident in lymphoid tissues and did not enter into circulation (Im et al., 2020). Importantly, the stem-like subset is essential for the maintenance of virus-specific CD8 T cell response during chronic infection and is responsible for the proliferative response of CD8 T cells observed after PD-1/PD-L1 checkpoint blockade (He et al., 2016; Im et al., 2016; Utzschneider et al., 2016).

These resource cells proliferate and initially give rise to a transitory population of T cell immunoglobulin mucin-3 (Tim3)+

[1]Emory Vaccine Center and Department of Microbiology and Immunology, Emory University School of Medicine, Atlanta, GA; [2]Winship Cancer Institute of Emory University, Atlanta, GA; [3]Department of Urology, Emory University School of Medicine, Atlanta, GA; [4]Laboratory of Immunoregulation and Mucosal Immunology, VIB-UGhent Center for Inflammation Research, Ghent University, Ghent, Belgium; [5]Department of Internal Medicine and Pediatrics, Ghent University, Ghent, Belgium; [6]Department of Microbiology, Immunology and Molecular Genetics, Long School of Medicine, University of Texas Health Science Center at San Antonio, San Antonio, TX; [7]Department of Dermatology, Hunan Key Laboratory of Medical Epigenomics, The Second Xiangya Hospital, Central South University, Changsha, Hunan, China; [8]Lymphocyte Biology Section, Laboratory of Immune System Biology, National Institute of Allergy and Infectious Diseases, National Institutes of Health, Bethesda, MD; [9]Genentech Inc., South San Francisco, CA.

Correspondence to R. Ahmed: rahmed@emory.edu.

cells by upregulating effector-like transcriptional signature (referred to as effector-like transitory subset; Hudson et al., 2019; Zander et al., 2019). The transitory cells downregulate the tissue retention marker CD69 and upregulate genes associated migration including *S1pr1, S1pr5,* and *Cx3cr1.* It is the major subset of antigen-specific CD8 T cells that enter into circulation during chronic infection (Hudson et al., 2019; Im et al., 2020; Zander et al., 2019). These transitory cells eventually differentiate into more terminally differentiated/exhausted cells expressing several inhibitory receptors including the glycoprotein CD101 . These exhausted cells (Tim3$^+$ CD101$^+$) are also resident and are found at major sites of chronic infection in both lymphoid and nonlymphoid tissues (Hudson et al., 2019; Im et al., 2020).

TGF-β is an immunosuppressive cytokine that regulates both innate and adaptive immune responses (Sanjabi et al., 2017). TGF-β initiates signaling pathways through binding to TGF-β type II receptor (TGF-βRII), which induces the formation of a tetrameric receptor complex consisting of two TGF-βRIIs and two TGF-βRIs. TGF-βRII phosphorylates and activates TGF-βRI, which then initiates the intracellular signaling pathway (Shi and Massagué, 2003). Extensive studies have examined how TGF-β regulates proliferation, apoptosis, differentiation, and localization of T cells (Batlle and Massagué, 2019). TGF-βRII deficiency results in selective accumulation of terminally differentiated effector T cells, and continuous TGF-β signaling is required for the maintenance of memory CD8 T cell phenotype after acute viral infection (Ma and Zhang, 2015). In addition, TGF-β induces expression of α$_E$β$_7$ integrin (CD103) and is essential for the generation and/or residence of tissue-resident memory T (T$_{RM}$) cells in many peripheral tissues (Schenkel and Masopust, 2014). A previous study showed that TGF-β signaling was increased in antigen-specific CD8 T cells during chronic LCMV infection compared with acute LCMV infection (Tinoco et al., 2009). Deletion of TGF-βRII on antigen-specific CD8 T cells or therapeutic blockade of TGF-β increased the numbers of antiviral T cells during LCMV clone 13 infection (Garidou et al., 2012; Tinoco et al., 2009). In addition, TGF-β signaling restricted proliferation and terminal differentiation of antiviral CD4 T cells and inhibited a cytotoxic program in CD4 T cells during chronic LCMV infection (Lewis et al., 2016). A recent study showed that TGF-β inhibited mammalian target of rapamycin (mTOR) signaling and preserved the metabolic fitness of stem-like antigen-specific CD8 T cells in chronically infected mice (Gabriel et al., 2021). There are also studies revealing TGF-β as an important player in immune suppression within the tumor microenvironment and examining the effects of TGF-β blockade in combination with PD-1/PD-L1 immune checkpoint therapy (Mariathasan et al., 2018; Tauriello et al., 2018). However, additional studies are needed to further elucidate the direct role of TGF-β signaling on regulating antigen-specific CD8 T cell differentiation during chronic infections and tumors.

In this study, we have examined the role of TGF-β in the differentiation and maintenance of different subsets of PD-1$^+$ antigen-specific CD8 T cells during chronic LCMV infection. We found that the expansion and durability of the transitory effector population was significantly increased in the absence of

TGF-β signaling. TGF-β restrained the differentiation of the stem-like subset into effector-like transitory cells by sustaining the unique transcriptional program of these cells, including upregulation of the stem-like cell-specific inhibitory receptors. In addition, TGF-β promoted the terminal differentiation/exhaustion of the transitory cells by suppressing effector- and proliferation-associated programs.

Results

Loss of TGF-β signaling promotes the differentiation of stem-like subset to effector-like transitory cells during chronic infection

To study the role of TGF-β signaling in directly regulating CD8 T cell responses during chronic infection, we used the following experimental setup. Transgenic P14 mice expressing TCR specific for LCMV GP33 epitope were crossed with mice with T cell–specific deletion of TGF-βRII mediated by Cre recombinase expressed under the control of distal Lck promoter (Pircher et al., 1990; Zhang and Bevan, 2012). CD44^{lo} naive TGF-βRII$^{fl/fl}$ (WT) and dLck-Cre$^+$ TGF-βRII$^{fl/fl}$ (knockout [KO]) P14 cells were harvested from donor mice expressing distinct congenic markers (CD45.1 or CD45.1/2) and then cotransferred in a 1:1 ratio into recipient C57BL/6 mice (CD45.2; Fig. 1 A). The recipient mice were then infected with LCMV clone 13 strain, and CD8 T cell responses were followed longitudinally during the early and late stages of chronic infection. This experimental approach enables direct comparison of WT and TGF-β receptor–deficient virus-specific CD8 cells (WT vs. KO P14 cells) differentiating in the same environment and in a WT recipient that had no deficiencies in the TGF-β pathway. Thus, any differences we observe in these two P14 cell populations would be due to direct (cell-intrinsic) TGF-β signaling.

We first compared the kinetics of CD8 T cell response between WT and TGF-β receptor–deficient P14 cells. The expansion of KO P14 cells was slightly reduced in the spleen during the first week of clone 13 infection, as shown by previous studies (Ma and Zhang, 2015; Zhang and Bevan, 2013). However, there were significantly increased numbers of KO P14 cells compared with WT P14 cells at later time points (Figs. 1 B and S1 A). The numbers of KO P14 cells also caught up with WT P14 cells in nonlymphoid tissues such as liver and lungs during chronic infection (Fig. S1, B and C). Therefore, the kinetics of CD8 T cell response suggest that TGF-βRII deletion resulted in an increase of virus-specific CD8 T cells from day 30 onward during chronic LCMV infection.

Next, we examined whether TGF-β signaling regulated the differentiation of antigen-specific CD8 T cells during chronic infection, and whether there were any changes in the generation and maintenance of the stem-like, transitory, and terminally differentiated subsets. TGF-βRII deficiency did not significantly alter the frequencies of the PD-1$^+$ TCF-1$^+$ Tim3$^-$ stem-like subset among WT and KO P14 cells in the spleen on day 5 and day 8 post-infection (D5 and D8 p.i.; Fig. 1, C and E; and Fig. S1, E and F). However, the frequencies of this subset were significantly reduced among KO P14 cells during the chronic stage of LCMV infection (Fig. 1, C and E; and Fig. S1 D). Still, due to increased
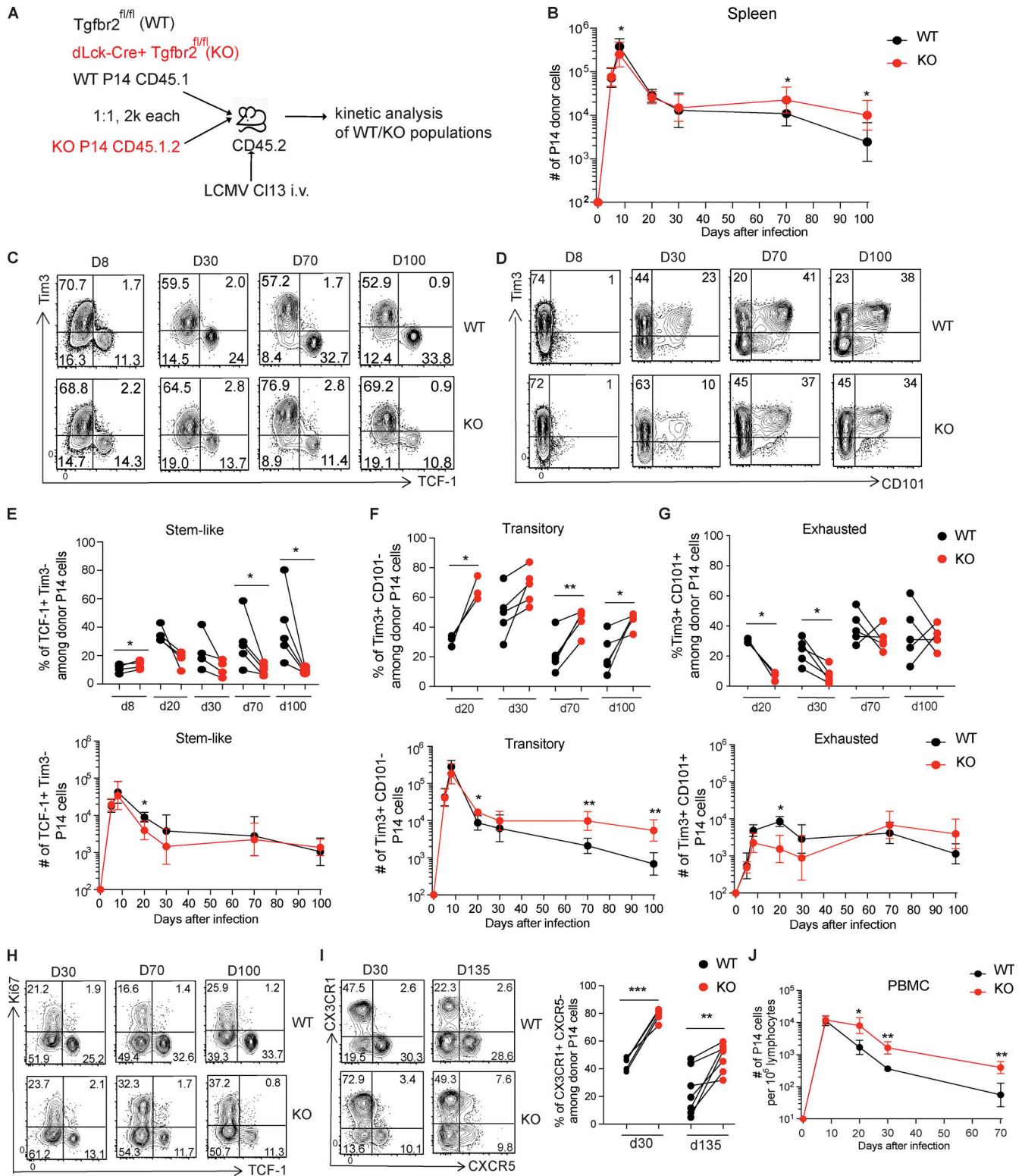
Figure 1. **TGF-β regulates the differentiation of different subsets of antigen-specific CD8 T cells during chronic LCMV infection. (A)** Congenically marked WT and TGF-βRII–deficient (KO) LCMV GP33-specific P14 CD8 T cells were cotransferred into naive mice treated with anti-CD4 depleting antibody GK1.5, followed by LCMV clone 13 infection. **(B)** Longitudinal analysis of the numbers of WT and KO P14 cells in the spleen. Graph shows the mean and SEM. Paired Student's t test; *, P < 0.05. **(C)** Representative FACS plots show the expression of Tim3 and TCF-1 by WT and KO P14 cells in the spleen at indicated time points. **(D)** Representative FACS plots show the expression of Tim3 and CD101 by WT and KO P14 cells in the spleen at indicated time points. **(E–G)** Frequencies and numbers of TCF-1+ Tim3− stem-like subset (E), Tim3+ CD101− transitory subset (F), and Tim3+ CD101+ exhausted subset (G) among WT and KO P14 cells in the spleen. Paired Student's t test; *, P < 0.05; **, P < 0.01. **(H)** Representative FACS plots show the expression of Ki67 and TCF-1 by WT and KO P14 cells in the spleen. **(I)** Representative FACS plots show the expression of CX3CR1 and CXCR5 by WT and KO P14 cells in the spleen (left). Graph shows

frequencies of of CX3CR1⁺ CXCR5⁻ transitory cells among WT and KO P14 cells at indicated time points (right). Paired Student's t test; **, $P < 0.01$; ***, $P < 0.001$. **(J)** Longitudinal analysis of the numbers of WT and KO P14 cells in the peripheral blood. Graph shows the mean and SEM. Paired Student's t test; *, $P < 0.05$; **, $P < 0.01$. PBMC, peripheral blood mononuclear cells. Data in B–J are representative of three independent experiments (n = 4–5 each time point per experiment).

total numbers of KO P14 cells at late time points (Fig. 1 B), there was no significant difference in the numbers of stem-like subset between WT and KO P14 cells (Fig. 1 E). During chronic LCMV infection, the TCF-1⁺ stem-like subset gives rise to Tim3⁺ CD101⁻ effector-like transitory cells, which undergo further differentiation into Tim3⁺ CD101⁺ exhausted subset (Hudson et al., 2019). We found that there were significantly increased frequencies and numbers of Tim3⁺ CD101⁻ transitory cells during chronic LCMV infection in the absence of TGF-β signaling (Fig. 1, D and F). The frequencies and numbers of Tim3⁺ CD101⁺ terminally differentiated subset were initially reduced by TGF-βRII deficiency but became comparable between WT and KO P14 cells at later time points (Fig. 1, D and G). Thus, the increased numbers of KO P14 cells at late time points were predominantly due to specific accumulation of the transitory cell population. Together, our data show that TGF-β signaling is not required for the initial generation of the TCF-1⁺ stem-like subset, but it inhibits the differentiation of these quiescent resource cells into an effector-like transitory subset during chronic LCMV infection.

In addition, significantly increased frequencies of KO P14 cells expressed Ki67, an indicator of cell proliferation, at later time points during chronic infection, which is consistent with enhanced differentiation into transitory cells in the absence of TGF-β signaling. The frequencies of Ki67⁺ cells among the stem-like subset were also increased on D30 p.i. in the absence of TGF-β signaling, which may indicate enhanced self-renewal (Figs. 1 H and S1 G). The transitory cells expressed the chemokine receptor CX3CR1 associated with migratory effector cells (Hudson et al., 2019; Zander et al., 2019), and entered into circulation during chronic infection (Im et al., 2020). Indeed, there were increased frequencies of CX3CR1⁺ cells among the KO P14 population compared with WT P14 cells (Fig. 1 I). Consistent with these phenotypic changes, TGF-βRII deletion resulted in significantly increased numbers of circulating P14 cells in peripheral blood at later time points (Fig. 1 J). The more differentiated KO P14 cells in the spleen harvested on D15 and D30 also showed increased production of IFN-γ compared with their WT counterparts upon in vitro stimulation with GP33 peptide (Fig. S1 H). These results confirm that loss of TGF-β signaling results in enhanced generation of circulating effector-like transitory cells during chronic infection.

RNA sequencing (RNA-seq) of LCMV-specific WT and KO P14 CD8 T cells shows increased levels of genes associated with transitory cells in the absence of TGF-β signaling

To further understand how TGF-β signaling regulates the differentiation of antigen-specific CD8 T cells during chronic LCMV infection, we examined the transcriptional changes induced by TGF-βRII deficiency in P14 cells. WT and KO P14 donor cells were sorted from spleens at different time points after LCMV clone 13 infection. The donor cells were further sorted

into Tim3⁺ CXCR5⁻ differentiated and CXCR5⁺ Tim3⁻ stem-like subsets (Fig. 2 A). RNA was extracted from sorted cells for RNA-seq.

Consistent with increased frequencies of transitory cells in absence of TGF-β signaling, Tim3⁺ KO P14 cells harvested on D15 p.i. showed increased transcription of several genes associated with effector T cells, e.g., *Cx3cr1*, *Il18rap*, and *Il12rb2*, compared with Tim3⁺ WT P14 cells. On the other hand, genes encoding inhibitory receptors, including *Cd200r1*, *Cd200r2*, and *Cd101*, were transcriptionally downregulated in the Tim3⁺ subset in the absence of TGF-β signaling. In addition, KLF2, the transcription factor associated with tissue exit (Carlson et al., 2006), was transcriptionally upregulated in Tim3⁺ KO P14 cells compared with Tim3⁺ WT counterparts ($\log_2$ fold-change = 0.75). There was also increased transcription of the target gene downstream of KLF2, *S1pr1* (Skon et al., 2013), in Tim3⁺ KO P14 cells. *S1pr5*, which mediates the tissue exit of NK cells (Jenne et al., 2009), was also transcriptionally upregulated in these cells (Fig. 2 B). These transcriptional differences between Tim3⁺ KO vs. WT P14 cells became much more significant on D30 p.i., when chronic infection was established. Similar to what we observed on D15 p.i., Tim3⁺ KO P14 cells upregulated the transcription of genes associated with effector differentiation and tissue exit (e.g., *Cx3cr1*, *Il12rb2*, *Il18rap*, *Klf2*, and *S1pr1*) and showed reduced expression of several inhibitory receptors including *Cd160*, *Cd101*, *Cd200r1*, and *Cd200r2* (Fig. 2, C and D). Flow cytometry validated the increased expression of IL18 receptor α (IL18Rα) and decreased expression of CD200 receptor on KO P14 cells on D30 (Fig. 2, E and F). Whereas the transcriptional profile of D15 Tim3⁺ KO P14 cells already showed positive enrichment for genes associated with the Tim3⁺ CD101⁻ transitory subset (Hudson et al., 2019), D30 Tim3⁺ KO P14 cells had stronger enrichment of the transitory subset signature. On the other hand, the gene signature of the Tim3⁺ CD101⁺ terminally differentiated subset (Hudson et al., 2019) was enriched in D15 and D30 Tim3⁺ WT P14 cells (Fig. 2 G). In addition, D15 and D30 Tim3⁺ KO P14 cells were enriched for circulating core genes (Milner et al., 2017), whereas their WT counterparts were enriched for residency core genes (Milner et al., 2017; Fig. 2 G). This is consistent with the fact that only the transitory subset was found in circulation, whereas both stem-like and terminally differentiated cells were tissue resident in this chronic infection model of lifelong viral persistence in multiple tissues (Im et al., 2020). Therefore, the transcriptional comparison of Tim3⁺ KO vs. WT P14 cells documents the enhanced generation of the transitory subset in the absence of TGF-β signaling.

TGF-β regulates the transcriptional signature of PD-1⁺ TCF-1⁺ stem-like subset

Next, we examined whether TGF-βRII deficiency altered the transcriptional profile of stem cell–like subset (Fig. 3 A). Only 27
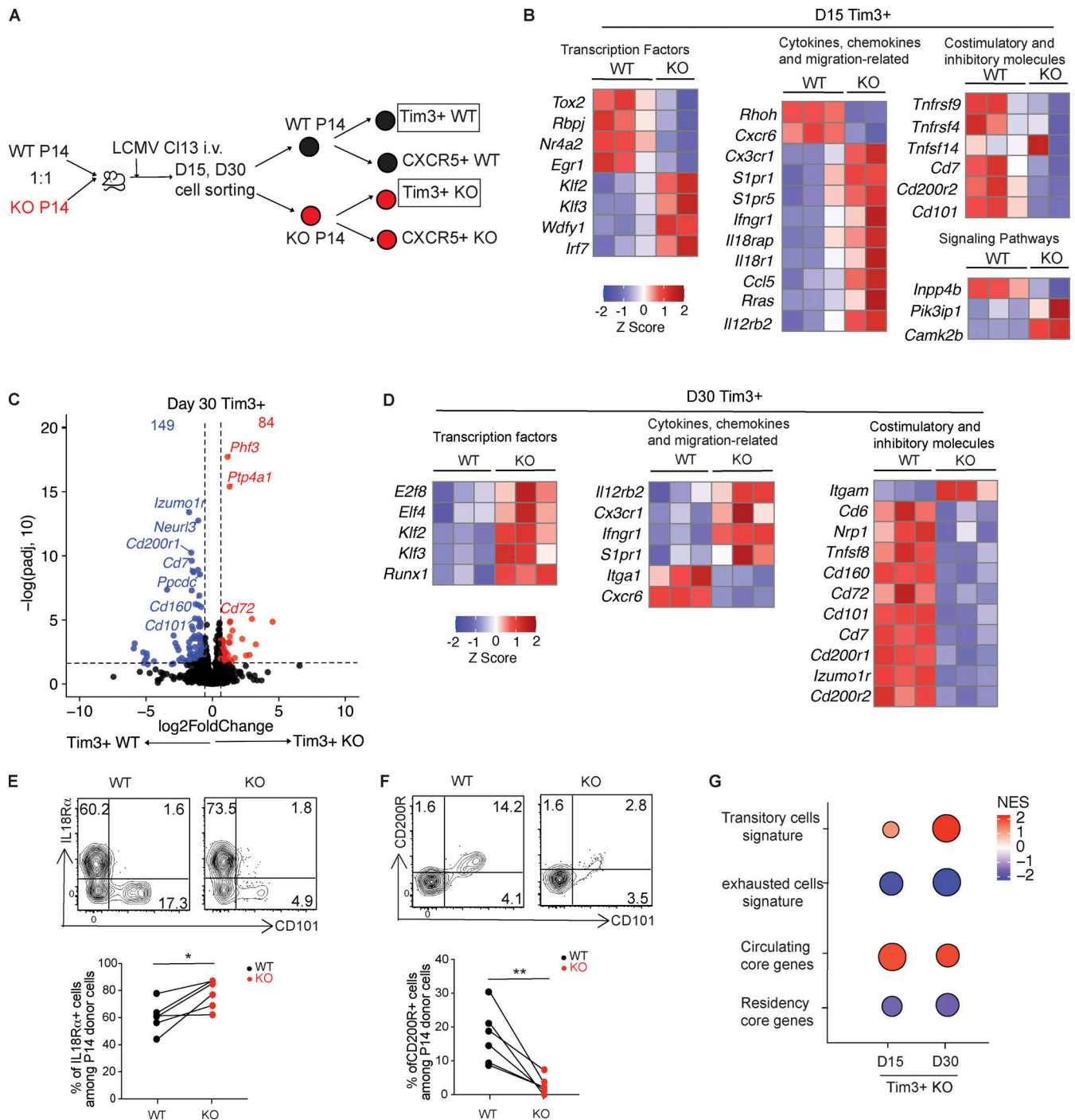
Figure 2. TGF-βRII deletion results in enhanced transcription of effector-associated genes in more differentiated antigen-specific CD8 T cells.
(A) Tim3+ CXCR5− differentiated cells were sorted from transferred KO and WT P14 cells in the spleen on D15 and D30 p.i. for RNA-seq. **(B)** Heatmap showing the relative expression (z-scores derived from expression values) of selected genes in Tim3+ KO vs. WT P14 cells on D15 p.i. **(C)** Volcano plots show $\log_2$ (fold-change) vs. $-\log_{10}$ (adjusted P value) of selected genes upregulated or downregulated in Tim3+ KO P14 cells compared with Tim3+ WT P14 cells on D30 p.i. The dotted lines indicates $\log_2$ (fold-change) = 0.6 or −0.6, and adjusted P = 0.05. **(D)** Heatmap showing the relative expression (z-scores derived from expression values) of selected genes in Tim3+ KO vs. WT P14 cells on D30 p.i. **(E and F)** Confirmation of increased expression of IL18Rα (E), and decreased expression of CD200R (F) on Tim3+ KO P14 cells by FACS. Paired Student's t test; *, P < 0.05; **, P < 0.01. **(G)** GSEA for enrichments of gene signatures of indicated cell types in D15 and D30 Tim3+ KO vs. WT P14 cells were visualized by NES and $-\log_{10}$ (FDR q value). RNA-seq datasets were generated from two to three biological replicates for each group at each time point.

genes (17 upregulated and 10 downregulated) were differentially transcribed in stem-like KO P14 cells >1.5-fold compared with stem-like WT P14 cells on D8 p.i. (normalized counts >50 in either stem-like WT or KO P14 cells, $\log_2$ fold-change >0.6 or <–0.6, adjusted $P < 0.05$; Fig. 3, B and C), consistent with the finding that loss of TGF-β signaling did not affect the generation of the stem-like subset. However, the transcriptional differences between stem-like KO and WT P14 cells continued to increase over time. On D15 p.i., 105 genes were differentially expressed in stem-like KO vs. WT cells (58 upregulated and 47 downregulated), and the number of differentially expressed genes further increased to 306 on D30 p.i. (146 upregulated and 160 downregulated; Fig. 3, B and C). On D15 p.i., stem-like KO P14 cells already showed reduced transcription of several genes specifically upregulated by stem cell–like WT P14 cells, such as *Itgb1*, *Sostdc1*, and *Cd200* (Fig. 3 B). On D30 p.i., TGF-βRII deletion resulted in reduced transcription of additional genes that were uniquely upregulated by stem cell–like WT P14 cells, including surface markers such as *Itgb1*, *Nt5e*, *Cd200*, *Cd83*, *Lrig1*, and *Art3* and transcription factors such as *Egr2* and *Id3* (Fig. 3 B). Indeed, GSEA showed that the transcriptional profiles of both D15 and D30 stem cell–like KO P14 cells were negatively enriched for the gene signature of stem cell–like subset (Fig. 3 D). These results show that TGF-β signaling directly on CD8 T cells plays an important role in regulating the transcriptional program specific for PD-1+ TCF-1+ stem-like cells during chronic infection.

It is of particular interest that the absence of TGF-β signaling led to reduced transcription of several inhibitory receptors/ligands that were uniquely upregulated by the stem-like subset but were not expressed by the more differentiated and exhausted CD8 T cells (Fig. 3 E). We confirmed by flow cytometry that CD73 (encoded by *Nt5e*) and CD200 were specifically upregulated by stem-like WT P14 cells, and their expression was reduced on stem-like KO P14 cells (Fig. 3 F). These inhibitory molecules have been shown to create an inhibitory environment (e.g., CD73; Regateiro et al., 2013) or to send inhibitory signal to antigen-presenting cells (e.g., CD200 and CD83; Chen et al., 2011; Eckhardt et al., 2014; Gorczynski, 2012; Horvatinovich et al., 2017). Stem-like KO P14 cells also showed reduced expression of NRP1, a checkpoint molecule limiting the self-renewal of stem-like cells (Liu et al., 2020), and the extracellular ATP-sensing purinergic receptor P2RX7, which promotes the metabolic fitness and survival of long-lived memory cells (Borges da Silva et al., 2018; Fig. 3, G and H). Specific upregulation of these inhibitory and stemness-associated molecules by stem cell–like subset suggests a possible mechanism by which the quiescence of these cells is maintained.

In addition, several transcription factors were expressed at reduced levels in stem-like KO P14 cells compared with stem-like WT P14 cells (Fig. 3 I). For example, stem-like KO P14 cells showed reduced transcription of early growth response 2 (EGR2) on D30 ($\log_2$ fold-change = –0.86), a transcription factor specifically upregulated by stem-like WT P14 cells (Wagle et al., 2021; Fig. 3 J). EGR2 is a direct target of nuclear factor of activated T cells (NFAT) signaling and serves as a negative regulator of T cell activation and function (Martinez et al., 2015; Williams et al., 2017). We confirmed decreased expression of EGR2 by

TCF-1+ stem-like KO P14 cells on D40 and D135 p.i. by flow cytometry (Fig. 3 J). EGR1, another EGR family member induced by NFAT (Collins et al., 2008), was also transcribed at reduced levels in D15 and D30 stem-like KO P14 cells (Fig. 3, B and I). EGR1 induced the expression of the phosphatase DUSP2, which led to loss of proliferative and effector capacities of tumor-infiltrating lymphocytes (Dan et al., 2020). Stem-like KO P14 cells also showed reduced transcription of *Dusp2* ($\log_2$ fold-change = –0.88) compared with their WT counterparts on D30 p.i. (Fig. 3 B). NFAT signaling plays a key role in CD8 T cell exhaustion by inducing transcription factors thymocyte selection-associated high mobility group (HMG) box (TOX), TOX2, and the nuclear receptor subfamily 4A (NR4A) family members (Alfei et al., 2019; Khan et al., 2019; Scott et al., 2019; Seo et al., 2019). Indeed, TOX2 was transcribed at reduced levels in D15 and D30 stem cell–like KO P14 cells (Fig. 3, B and I). Gene set enrichment analysis (GSEA) showed that NFAT target genes in exhausted CD8 T cells (Martinez et al., 2015) were negatively enriched in the transcription profiles of D15 and D30 stem-like KO cells (Fig. 3 K). Therefore, TGF-β signaling may maintain the stemness of these resource cells by regulating key transcriptional regulators. Together, these data suggest that TGF-β signaling transcriptionally maintains the gene signature of stem-like cells during chronic infection.

Single-cell RNA-seq (scRNA-seq) of WT and TGF-βRII–deficient P14 cells from chronically infected mice

We further examined how TGF-β signaling regulated the transcriptional profile of virus-specific CD8 T cells at the single-cell level. WT and KO P14 cells were sorted from spleen on D30 p.i. for scRNA-seq (Fig. 4 A). Uniform Manifold Approximation and Projection (UMAP) clustering identified three transcriptionally distinct clusters in both KO and WT samples (Fig. 4 B), and overlay of the UMAP analyses suggested similar distribution of WT and KO P14 cells (Fig. 4 C). We performed GSEA on these cells using signatures for stem (Tim3− CD101−), transitory (Tim3+ CD101−), and exhausted (Tim3+ CD101+) CD8 T cells defined in previous work (Hudson et al., 2019). Based on the enrichment of gene signatures in each cluster (Fig. S2 A), we referred to the three clusters of WT and KO cells as stem, transitory, and exhausted (Figs. 4 B and S2 A). Importantly, there was no significant difference in enrichment scores between WT and KO, suggesting similar differentiation processes in both these cells (Fig. S2 A).

When we looked at specific genes expressed by each cluster, canonical markers of exhausted CD8 T cell subsets were detected. *Pdcd1* and *Tox*, the characteristic genes of CD8 T cell exhaustion, were expressed by all cells. Cells in the stem-like cluster showed selectively high expression of *Tcf7*, *Slamf6*, *Il7r*, *Sell*, and *Id3*, the key genes associated with stem-like subset during chronic infection. Both transitory and exhausted clusters expressed *Havcr2* (Tim3). The cells in the transitory cluster were characterized by elevated expression of genes associated with effector differentiation and tissue exit, including *Cx3cr1*, *Il18rap*, *S1pr1*, *S1pr5*, *Ifngr1*, *Gzmb*, *Ifng*, *Tbx21*, *Zeb2*, *Prdm1*, and *Klf2*, consistent with the transcriptional signature of transitory subset. The cells in exhausted cluster downregulated these effector-
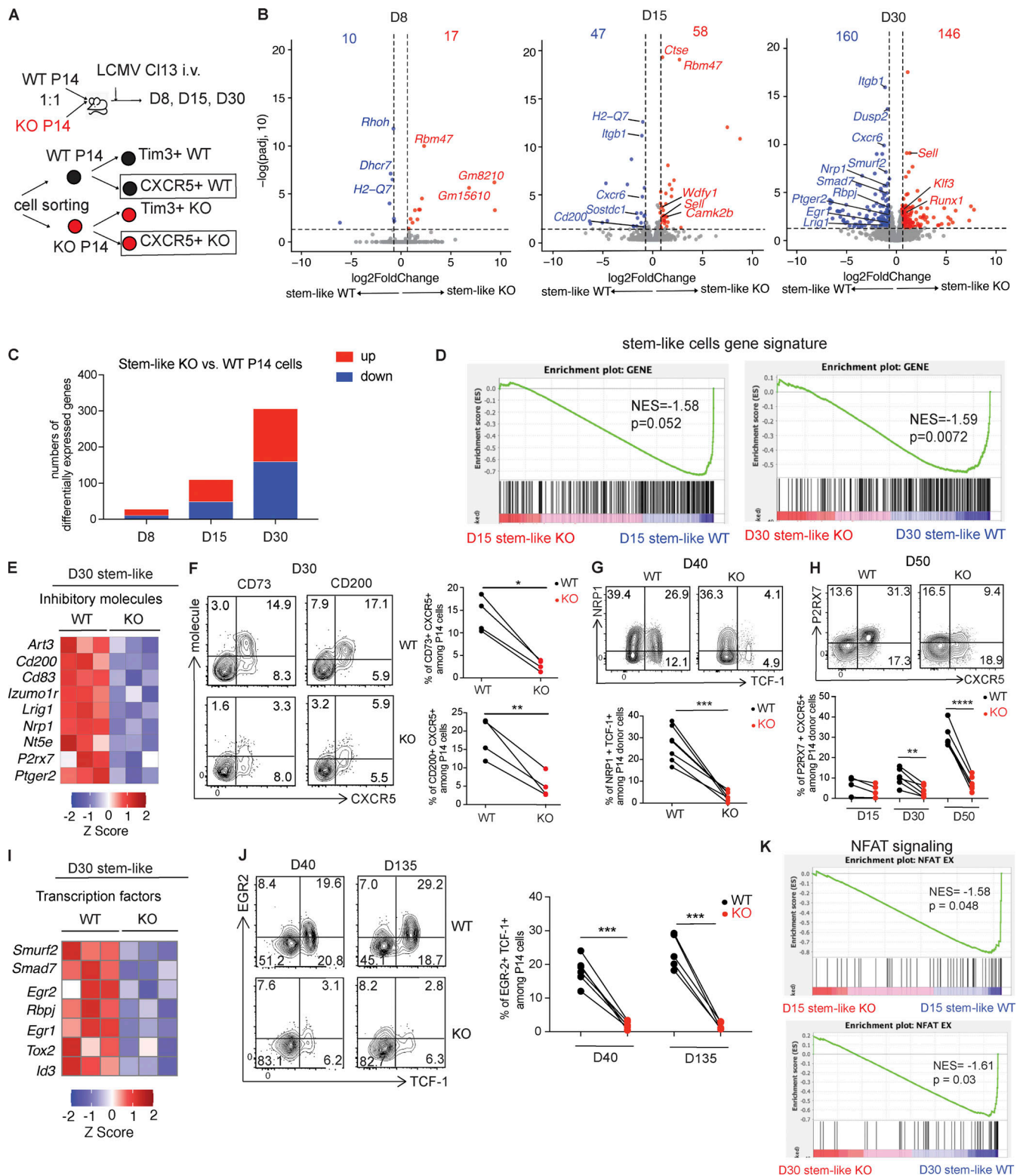
Figure 3. **TGF-β signaling regulates the transcriptional signature of stem-like subset during chronic infection. (A)** CXCR5+ Tim3− stem-like cells were sorted on D8, D15, and D30 p.i. from transferred WT and KO P14 cells in the spleen for RNA-seq. **(B)** Volcano plots show log₂ (fold-change) vs. −log₁₀ (adjusted P value) of genes upregulated or downregulated in stem-like KO P14 cells compared with stem-like WT P14 cells at indicated time points. The dotted line indicates log₂(fold-change) = 0.6 or −0.6, and adjusted P = 0.05. **(C)** Numbers of differentially expressed genes between stem-like KO vs. WT P14 cells at indicated time points (log₂[fold-change] >0.6 or <−0.6, adjusted P < 0.05). **(D)** GSEA compared genes uniquely upregulated in stem-like subset with the transcriptional profiles of stem-like KO vs. WT P14 cells on D15 and D30 p.i. **(E)** Heatmap showing the relative expression (z-scores derived from expression values) of selected inhibitory molecules in stem-like KO vs. WT P14 cells on D30 p.i. **(F)** Representative FACS plots confirm reduced expression of CD73 and CD200 on stem-like KO P14 cells compared with stem-like WT P14 cells in the spleen on D30 p.i. (left). Frequencies of CD73+ CXCR5+ cells and CD200+ CXCR5+

cells among WT and KO P14 cells on D30 p.i. (right). Paired Student's *t* test; *, P < 0.05; **, P < 0.01. **(G)** Representative FACS plots confirm reduced expression of NRP1 on stem-like KO P14 cells compared with stem-like WT P14 cells in the spleen on D40 p.i. (upper). Frequencies of NRP1⁺ TCF-1⁺ cells among WT and KO P14 cells on D40 p.i. (lower). Paired Student's *t* test; ***, P < 0.001. **(H)** Representative FACS plots confirm reduced expression of P2RX7 on stem-like KO P14 cells compared with stem-like WT P14 cells in the spleen on D50 p.i. (upper). Frequencies of P2RX7⁺ CXCR5⁺ cells among WT and KO P14 cells at indicated time points (lower). Paired Student's *t* test; **, P < 0.01; ****, P < 0.0001. Data in F–H are representative of two independent experiments with four to seven mice per time point per experiment. **(I)** Heatmap showing the relative expression (*z*-scores derived from expression values) of selected transcription factors in stem-like KO vs. WT P14 cells on D30 p.i. **(J)** Representative FACS plots show EGR2 expression on TCF-1⁺ WT and KO P14 cells in the spleen on D40 and D135 p.i. (left). Frequencies of EGR2⁺ TCF-1⁺ cells among WT and KO P14 cells at indicated time points (right). Paired Student's *t* test; ***, P < 0.001. **(K)** GSEA showed that NFAT target genes in exhausted CD8 T cells were negatively enriched in stem-like KO P14 cells on D15 and D30 p.i. RNA-seq datasets were generated from two to three biological replicates for each group.

associated genes but upregulated genes encoding inhibitory receptors such as *Cd101*, *Cd200r1*, *Cd244*, and *Tigit* (Figs. 4 D and S3 B). While there was no major difference in the clusters identified between WT and KO CD8 T cells, there were significant changes in the relative proportion of each cluster. There was increased frequency of transitory and decreased frequencies of stem and exhausted in KO P14 cells compared with WT P14 cells, consistent with what we observed by flow cytometry at the population level (Fig. 4 E). Interestingly, there seemed to be two subclusters within the transitory cluster, with higher frequencies of KO cells in both subclusters (Fig. 4 E). One subcluster (green dashed circle in Fig. 4 E) may suggest a pre-exhaustion state with downregulation of migration and effector-related genes such as *Cx3cr1*, *S1pr5*, and *Tbx21* (Figs. 4 D and S3 B).

Taken together, the results of the scRNA-seq analysis further extend the phenotypic data (Fig. 1) and clearly document an increase in the transitory effector LCMV-specific CD8 T cells in the absence of TGF-β signaling during chronic LCMV infection.

Conditional deletion of TGF-β receptor from LCMV-specific P14 CD8 T cells during established chronic infection results in increased generation of effector-like transitory cells

Next, we used a model of conditional deletion of TGF-βRII to further confirm the roles of TGF-β signaling in CD8 T cell response during chronic LCMV infection. Here we crossed loxP-flanked TGF-βRII (TGF-βRII^fl/fl) mice to Rosa26Cre-ERT2 (ER-Cre) mice to enable the deletion of TGF-βRII upon tamoxifen (TAM) treatment, and these mice were crossed to P14 transgenic mice for transfer experiment. In this experiment, naive P14 cells from ER-Cre⁺ TGF-βRII^fl/fl (Tgfbr2^fl/fl) and ER-Cre⁺ TGF-βRII^+/+ (WT) littermates were cotransferred into naive B6 mice, which were then chronically infected with LCMV clone 13. Recipient mice were treated with TAM to induce the deletion of TGF-βRII ~1 mo p.i., when the chronic infection was established (Fig. 5 A). 25 d after TAM treatment, on D60 p.i., frequencies of TCF-1⁺ Tim3⁻ stem-like subset were significantly reduced among Tgfbr2^fl/fl P14 cells compared with WT P14 cells in mice treated with TAM, whereas the frequencies of Ki67⁺ cells were significantly increased, which suggests enhanced differentiation and proliferation resulting from inducible TGF-βRII deletion (Fig. 5, B–E). Consistent with this, the frequencies of the transitory subset, as shown by their Tim3⁺ CD101⁻ and CX3CR1⁺ TCF-1⁻ phenotype, were significantly increased among Tgfbr2^fl/fl P14 cells in TAM-treated mice (Fig. 5, F and G). Therefore, conditional deletion of TGF-βRII led to enhanced generation of transitory cells, showing that TGF-β signaling is constantly required

to restrain the differentiation of stem-like subset during chronic infection.

TGF-β contributes to the immunosuppressive environment of an established chronic infection

In earlier experiments (Fig. 1), when WT and KO P14 cells were transferred into naive recipients followed by LCMV clone 13 infection, the regulatory effects of TGF-β on antigen-specific CD8 T cells were more evident in the later stages of infection. To address this more directly, we compared the response of WT P14 cells after transfer into established chronically infected mice (>D45 p.i.) vs. transfer into naive mice followed by LCMV clone 13 infection. When WT P14 cells were transferred into established chronically infected mice, their numbers at the peak of the expansion were greatly reduced (~100-fold) in all tissues compared with the experimental setting, when they were transferred into naive mice followed by clone 13 infection (Fig. S3 A). These data show that the chronic environment is immunosuppressive for T cell expansion.

We then examined whether TGF-β was playing a role in the suppressed expansion of antigen-specific CD8 T cells activated in established chronic LCMV infection. To address this question, we cotransferred congenically marked naive WT P14 cells and KO P14 cells into recipient mice with established LCMV chronic infection (>D45 p.i.), and monitored their expansion and differentiation longitudinally (Fig. 6 A). The results were quite striking, with significantly increased frequencies and numbers of KO P14 cells compared with WT P14 cells in all tissues analyzed (Fig. 6, B and C). The ratio of KO vs. WT P14 cells was much higher compared with the setting when P14 cells were primed at the onset of the infection (Fig. S3 B). These results demonstrate that TGF-β strongly inhibits the expansion of antigen-specific CD8 T cells in the immunosuppressive environment of established chronic infection. Consistent with this, the frequencies and numbers of Tim3⁺ CD101⁻ transitory CD8 T cell subset were significantly increased among KO P14 cells (Fig. 6, D–H). Also, there were increased frequencies of KO P14 cells expressing Ki67 (Fig. S3 C). These results show that loss of TGF-β signaling potently enhances the differentiation of virus-specific CD8 T cells activated in established chronic LCMV infection.

We also used the model of conditional deletion of TGF-βRII to rule out the impact of any preinfection differences between WT and KO P14 cells. ER-Cre⁺ Tgfbr2^WT/WT and ER-Cre⁺ Tgfbr2^flox/flox P14 cells were cotransferred into chronically infected mice, and the recipient mice were treated with TAM from day 0 to day 4 after transfer to delete TGF-βRII (Fig. S3 D).
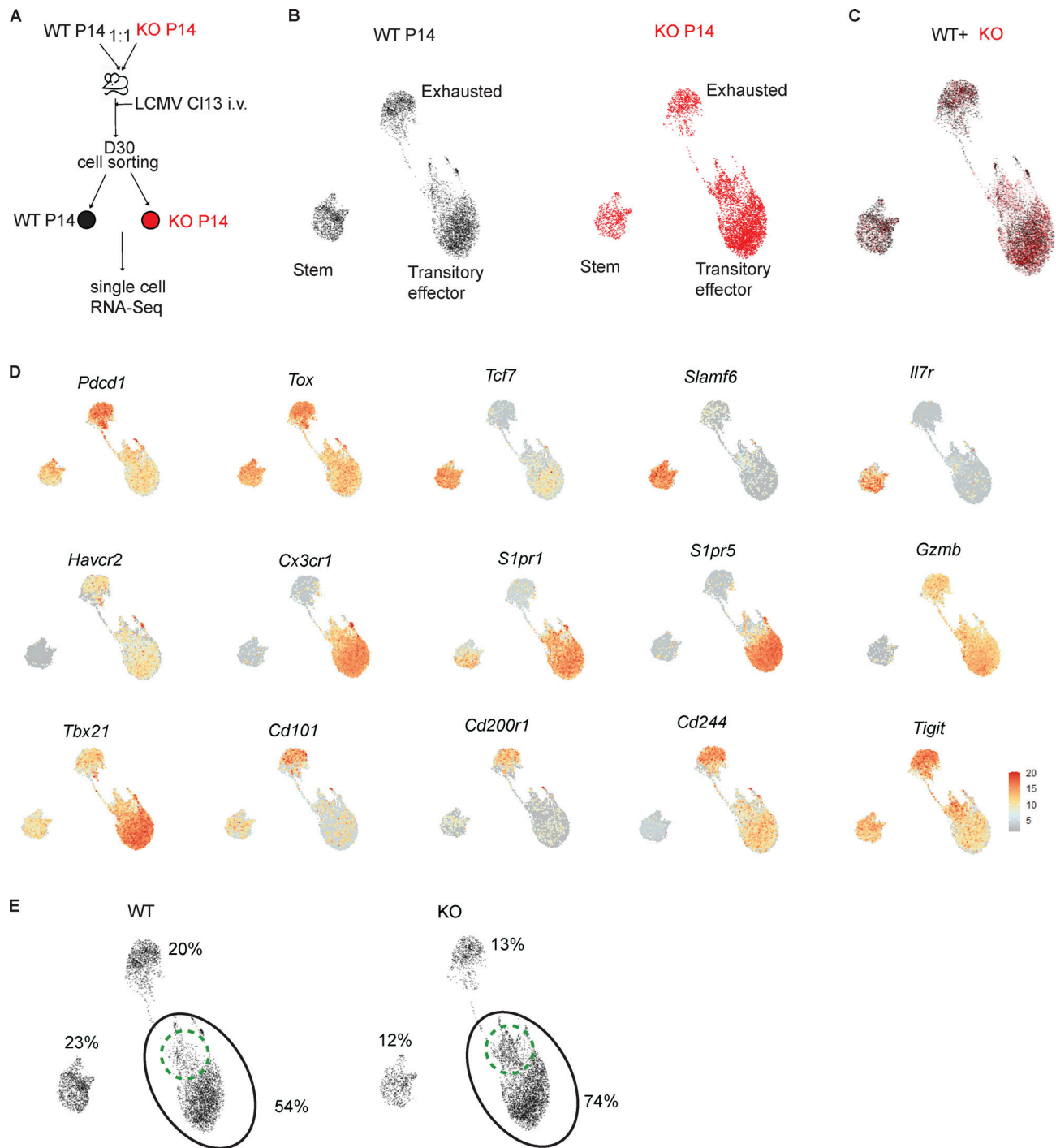
Figure 4. **scRNA-seq of WT and TGF-βRII–deficient P14 cells from chronically infected mice. (A)** Congenically marked WT and TGF-βRII–deficient (KO) P14 CD8 T cells were cotransferred into naive mice treated with anti-CD4 depleting antibody GK1.5, followed by LCMV clone 13 infection. WT and KO P14 cells were sorted from spleen on D30 p.i. for scRNA-seq. **(B)** UMAP analyses identified three distinct clusters for both WT and KO P14 cells: stem-like, transitory, and exhausted. **(C)** An overlay of WT (black) and KO (red) UMAP analyses. **(D)** UMAP plots showing the expression of selected genes. **(E)** The frequencies of WT and KO P14 cells in the stem, transitory, and exhausted clusters, with two subclusters identified within the transitory cluster. The green dotted line circles the subcluster at possible pre-exhaustion state.

Similar to what we observed from the transfer of KO/WT P14 cells, there was also significantly increased accumulation of Tgfbr2$^{flox/flox}$ P14 cells compared with WT P14 cells on D15 after transfer (Fig. S3 E), and conditional deletion of TGF-βRII also resulted in significantly increased frequencies of transitory cells

(Fig. S3 F). These results showed that the phenotypic differences that we observed in Fig. 6 was not due to any developmental changes in the KO P14 cells.

We next examined whether TGF-β regulated the anatomic location of P14 cells primed in chronically infected mice.
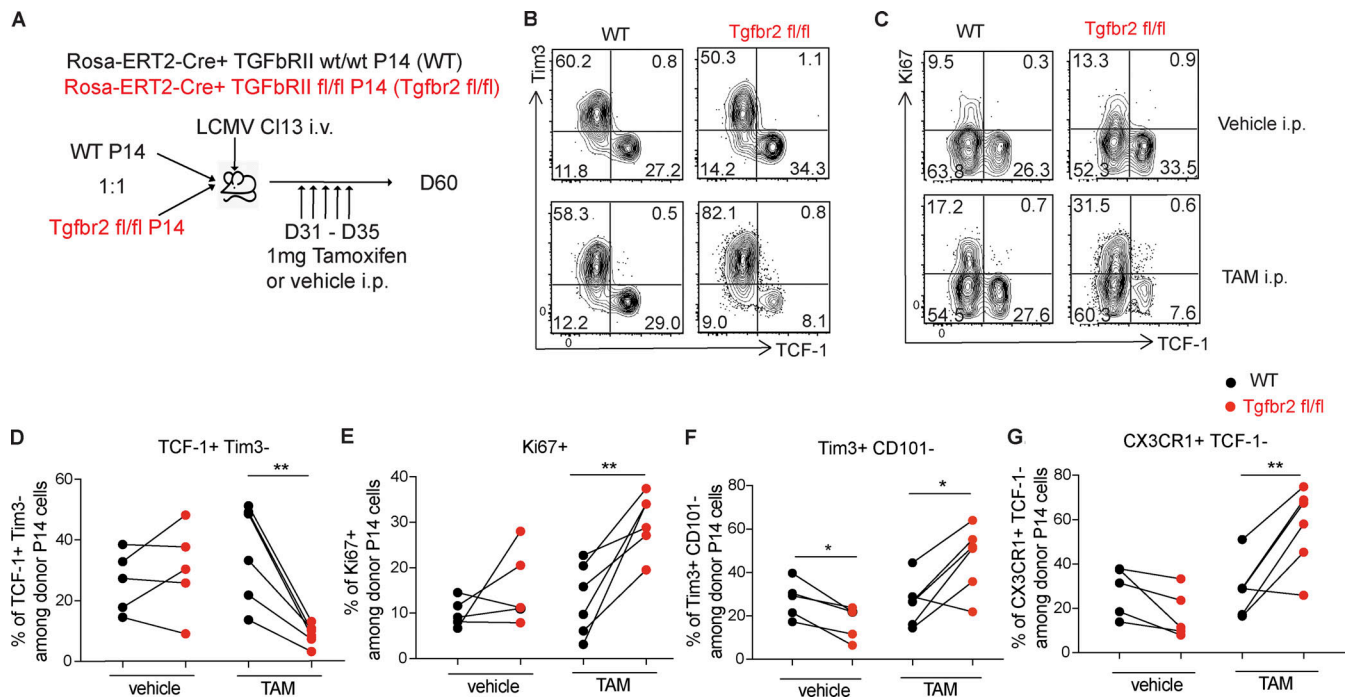
Figure 5. TGF-β signaling is continuously needed to inhibit differentiation of antigen-specific CD8 T cells during chronic LCMV infection. **(A)** Rosa26Cre-ERT2+ TGF-βRII^fl/fl (Tgfbr2^fl/fl) and Rosa26Cre-ERT2+ TGF-βRII^+/+ (WT) P14 cells were cotransferred into naive B6 mice with CD4 T cell depletion and were then infected with LCMV clone 13. Recipient mice were treated with TAM or vehicle for 5 consecutive days (D31–D35 p.i.) to induce the deletion of TGF-βRII. Donor cells were harvested from spleen on D60 p.i. Representative FACS plots show the expression of Tim3 and TCF-1 (B) or Ki67 and TCF-1 (C) by Tgfbr2^fl/fl and WT P14 cells from mice treated with vehicle or TAM. **(D–G)** Plots show frequencies of TCF-1+ Tim3− (D), Ki67+ (E), Tim3+ CD101− (F), and CX3CR1+ TCF-1− (G) cells among WT and Tgfbr2^fl/fl P14 cells in the spleen. In D–G, paired Student's t test; *, P < 0.05. **, P < 0.01. Data in B–G are representative of two independent experiments (n = 5–6 each time point per experiment).

Histocytometry confirmed that TGF-βRII deletion increased the frequencies of P14 cells localized to the red pulp of the spleen on D20 after transfer (Fig. S4, A and B). This is due to preferential localization of TCF-1–negative differentiated KO P14 cells to the red pulp compared with differentiated WT P14 cells, whereas the TCF-1+ stem-like WT and KO P14 cells were mostly located in the T cell zones (Fig. S4 C).

To further understand the inhibitory roles of TGF-β on the expansion and differentiation of CD8 T cells primed in chronically infected mice, we compared the transcriptional profiles of WT and KO P14 cells on D12 after transfer via RNA-seq (Fig. 7 A). 127 genes had significant differential expression between WT and KO P14 cells (normalized counts >50 in either WT or KO P14 cells, log2 fold-change >0.6 or <−0.6, adjusted P < 0.05; Fig. 7 B and Fig. S5). GSEA identified positive enrichment of biological pathways associated with T cell activation in KO P14 cells compared with WT P14 cells, including antigen response, cell cycle progression, mammalian target of rapamycin complex 1 (mTORC1) signaling, and DNA replication (Fig. 7 C). Indeed, KO P14 cells upregulated transcription of several genes associated with mTOR signaling and glycolysis, including Slc2a3, Slc2a1, Hk2, Ldha, and Hif1a (Fig. 7 D). We confirmed that KO P14 cells showed increased phosphorylation of S6 ribosome protein downstream of mTOR signaling (Fig. 7 E). We also observed upregulation of genes associated with effector differentiation in KO P14 cells activated in chronically infected mice, including transcription factors such as Zeb2, Bhlhe40, Tbx21, and Id2; surface markers such as Klrg1, Klre1,

Il12rb2, Il18rap, S1pr5, and Cx3cr1; and effector molecules such as Gzma, Prf1, and Ifng (Figs. 7 F and S5; Joshi et al., 2007). We confirmed by flow cytometry that higher frequencies of KO P14 cells expressed effector cell marker killer cell lectin-like receptor G1 (KLRG1) on D15 after transfer (Fig. 7 G). Subsets of KO P14 cells also showed increased production of IFN-γ and TNF upon in vitro stimulation compared with their WT counterparts (Fig. 7 H). On the other hand, KO P14 cells showed reduced transcription of genes associated with memory CD8 T cells and stem-like CD8 T cells, including Id3, Tcf7, Il7r, and Xcl1 (Im et al., 2016; Joshi et al., 2007) and downregulated the transcription of several inhibitory receptors, including Cd200r1, Cd101, Nrp1, and Ctla4 (Fig. S5). Consistent with KO P14 cells primed at the onset of the infection, KO P14 cells activated in established chronic infection were also positively enriched for gene signature of transitory cells (Hudson et al., 2019) and circulating core genes (Milner et al., 2017) and were negatively enriched for gene signature of terminally differentiated cells (Hudson et al., 2019) and residency core genes (Milner et al., 2017; Fig. 7 I). Together, these results suggest that TGF-β suppresses the expansion and differentiation of virus-specific CD8 T cells primed in chronically infected mice by inhibiting the effector-associated transcriptional program.

Adoptive transfer of stem-like and transitory subsets into chronically infected mice
We performed adoptive transfer experiments to examine the effects of TGF-β on different subsets of P14 cells during chronic

Hu et al.
TGF-β regulates CTLs during chronic infection

Journal of Experimental Medicine   10 of 21
https://doi.org/10.1084/jem.20211574
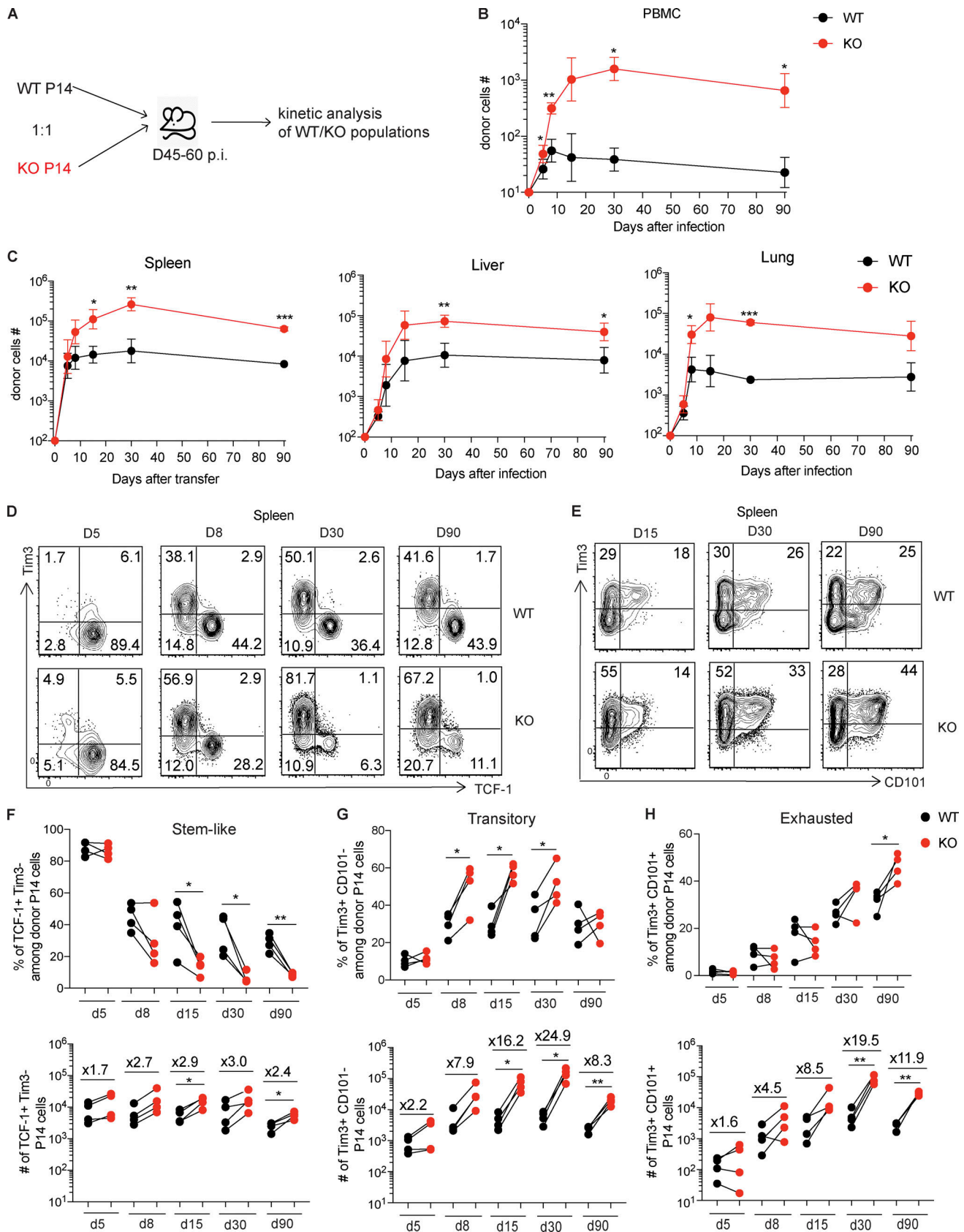
Figure 6. **TGF-β suppresses the differentiation of antigen-specific CD8 T cells activated in an established chronic infection. (A)** Congenically marked WT and KO P14 cells were cotransferred into mice chronically infected with LCMV clone 13 (D45–D60 p.i.). **(B)** Longitudinal analysis showed the numbers of WT and KO P14 cells in the peripheral blood. **(C)** Longitudinal analysis of the numbers of WT and KO P14 cells in the spleen, liver, and lungs. Graph shows the

Hu et al.
TGF-β regulates CTLs during chronic infection

Journal of Experimental Medicine   11 of 21
https://doi.org/10.1084/jem.20211574

mean and SEM. In B and C, paired Student's *t* test; *, P < 0.05; **, P < 0.01; ***, P < 0.001. **(D)** Representative FACS plots show the expression of Tim3 and TCF-1 by WT and KO P14 cells in the spleen at indicated time points after transfer. **(E)** Representative FACS plots show the expression of Tim3 and CD101 by WT and KO P14 cells in the spleen at indicated time points after transfer. **(F–H)** Frequencies and numbers of TCF-1$^+$ Tim3$^-$ stem-like subset (F), Tim3$^+$ CD101$^-$ transitory subset (G), and Tim3$^+$ CD101$^+$ exhausted subset (H) among WT and KO P14 cells in the spleen. Paired Student's *t* test; *, P < 0.05; **, P < 0.01. Data in B–H are representative of three independent experiments (*n* = 4–5 each time point per experiment).

infection. We sorted the stem-like subset (PD-1$^+$ Slamf6$^+$ Tim3$^-$ CXRCR1$^-$) from WT and TGF-βRII KO P14 cells on D10 after clone 13 infection, mixed these WT and KO stem-like P14 cells at a 1:1 ratio, and adoptively transferred them into established chronically infected mice (>D45 p.i.; Fig. 8 A). Another group of chronically infected mice received a 1:1 mixture of sorted WT and KO P14 transitory effector CD8 T cells (PD-1$^+$ Tim3$^+$ Slamf6$^-$ CD101$^-$; Fig. 8 B). Appropriate congenic markers were used to distinguish the WT and KO P14 cells from each other and from the endogenous CD8 T cells in the recipient mouse (Fig. 8, A and B). The KO P14 stem-like subset expanded significantly more than the WT P14 counterparts; the starting ratio was 1:1, but 9 d after transfer into the chronically infected mice the KO P14 cells dominated by a >4:1 ratio in the spleen (Fig. 8 C). The KO transitory effector subset showed a similar pattern but to a lesser extent (Fig. 8 D). The results of these adoptive transfer experiments using sorted populations of the subsets show that the expansion of both the stem-like and transitory subsets is regulated by TGF-β signaling during chronic LCMV infection.

We next asked what the differentiation trajectory of the WT and KO stem-like P14 cells was after transfer into the chronically infected mice. The purity of the sorted stem-like cells from WT and KO P14 LCMV-specific CD8 T cells is shown in Fig. 8 E, and the differentiation results are shown in Fig. 8, F–H. As expected the stem-like CD8 T cells gave rise to the more differentiated Tim-3$^+$ CD8 T cells. This differentiation pattern was seen for both the WT and KO stem-like P14 cells and is indicated by the solid green arrow (Fig. 8 F). Thus, both WT and KO stem-like P14 cells behave similarly in this aspect. However, interesting differences were seen in the differentiation of WT and KO stem-like cells into the transitory effector and the more terminally differentiated/exhausted CD101$^+$ CD8 T cell subsets. We found that there were a significantly higher proportion of transitory effector CD8 T cells and a lower proportion of exhausted CD8 T cells in KO P14 cells compared with the WT P14 cells (Fig. 8, G and H). Thus, the differentiation trajectory shows that both the WT and KO P14 stem-like cells differentiate into the transitory effector CD8 T cells (solid green arrow), but the frequency of transitory effector cells is greater with the TGF-βRII KO cells (Fig. 8, G and H). Also, there are significantly fewer exhausted CD8 T cells in the absence of TGF-β signaling. These terminally differentiated CD101$^+$ CD8 T cells could have emerged from the transitory effector population or from the stem-like CD8 T cells directly; hence these trajectories are shown as dotted green lines (Fig. 8 G).

To get a better understanding of the differentiation trajectories, we next examined differentiation of the WT and KO transitory effectors cells after transfer into the chronically infected mice. The sorting strategy and purity of the transitory effector subsets are shown in Fig. 8 I, and the results are shown in Fig. 8, J–N. As expected, the transitory effector WT or KO P14

cells did not revert back into becoming stem-like CD8 T cells under the conditions of a chronic infection (Fig. 8 J). However, the transitory effector CD8 T cells clearly gave rise to the terminally differentiated subset, and this was seen with both WT and KO P14 cells (Fig. 8 K, solid green lines). The most striking difference between the WT and KO transitory effector cells once again was the slower differentiation into the exhausted CD8 T cell subset in the absence of TGF-β signaling (Fig. 8, K and I). Thus, there were higher proportions of transitory effector cells and lower frequencies of CD101$^+$ exhausted CD8 T cells in KO vs. WT P14 cells. This pattern of differentiation was seen not only in the spleens of the chronically infected recipient mice after adoptive transfer but also in nonlymphoid tissues such as liver and lung of these recipient mice (Fig. 8, M and N).

Based on the results seen after the adoptive transfer of the stem-like cells and the transitory effector cells, the most likely differentiation trajectory for both WT and KO P14 CD8 T cells during chronic infection is stem to transitory effector to exhausted cells. These results also document that TGF-β signaling plays an important role in regulating this CD8 T cell differentiation pathway during chronic infection.

Treatment of chronically infected mice with anti–TGF-β blocking antibody enhances the generation of virus-specific transitory CD8 T cells

Previous studies showed that antibody blockades of TGF-β signaling during LCMV clone 13 infection increased the numbers of antigen-specific CD8 T cells (Boettler et al., 2012; Garidou et al., 2012). Here we further examined whether blocking TGF-β signaling in chronically infected mice had similar effects on the expansion and differentiation of antigen-specific CD8 T cells as genetic deletion of TGF-βRII. Mice chronically infected with LCMV clone 13 (>D45 p.i.) were treated with anti–TGF-β antibody or isotype control every other day for 2 wk (Fig. 9 A). TGF-β blockade led to significantly increased numbers of CD8 T cells specific for GP33 and GP276 epitopes (Fig. 9 B). Blocking TGF-β signaling also resulted in increased frequencies of Ki67$^+$ cells among GP33-specific and GP276-specific CD8 T cells, which suggests significantly enhanced proliferation of antigen-specific CD8 T cells (Fig. 9, C and D). Consistently, we observed increased frequencies of the Tim3$^+$ CD101$^-$ transitory cells among GP33-specific and GP276-specific CD8 T cells after TGF-β blockade (Fig. 9, E and F). Together, these results show that blocking TGF-β signaling enhanced antigen-specific CD8 T cell response during chronic infection by increasing cell proliferation and the generation of transitory cells.

Discussion
The main findings of our study are summarized in Fig. 10. Panel A shows the dynamics of the WT and TGF-βRII KO P14 CD8 T cell

Hu et al.
TGF-β regulates CTLs during chronic infection

Journal of Experimental Medicine   12 of 21
https://doi.org/10.1084/jem.20211574
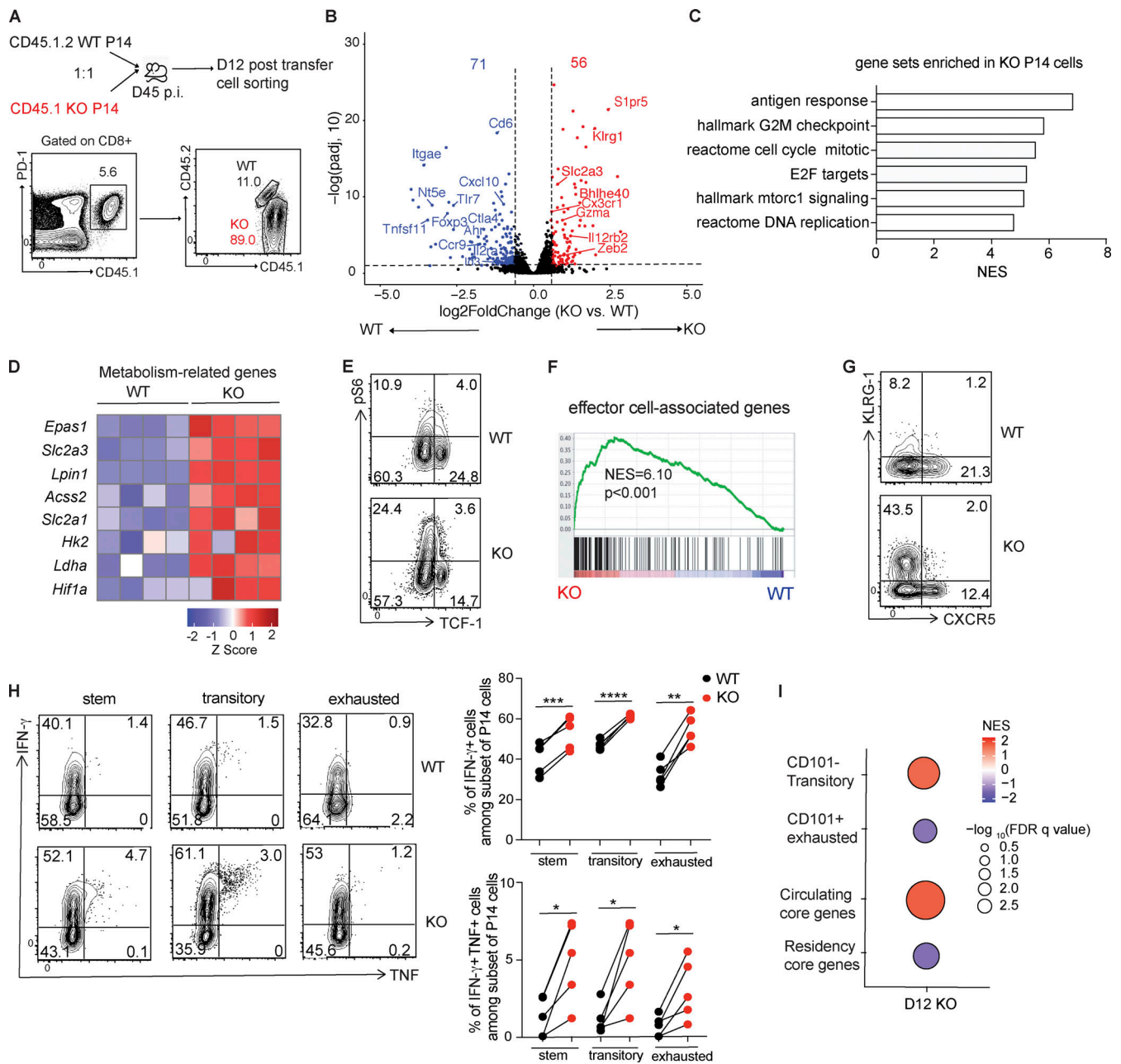
Figure 7. **Transcriptional analysis of WT and TGF-β receptor–deficient antigen-specific CD8 T cells activated in chronically infected mice. (A)** Graph showing the experimental design of RNA-seq. **(B)** Volcano plots show $\log_2$(fold-change) vs. $-\log_{10}$ (adjusted P value) of selected genes upregulated or downregulated in KO P14 cells compared with WT P14 cells on D12 after transfer into mice with established chronic LCMV infection. The dotted lines indicate $\log_2$(fold-change) = 0.6 or −0.6, and adjusted P = 0.05. **(C)** GSEA shows biological pathways enriched in KO P14 cells activated in mice with established chronic LCMV infection. Plotted by NES. **(D)** Heatmap showing the relative expression of metabolism-related genes in KO vs. WT P14 cells. Heatmaps generated using z-scores derived from normalized counts. **(E)** Representative FACS plots showed phosphorylation of S6 ribosome protein ex vivo on D15 after transfer. **(F)** GSEA-compared gene signatures of IL-7R^{lo} effector cells on D8 after acute LCMV Armstrong infection for enrichment in the transcriptional profiles of KO vs. WT P14 cells. **(G)** Representative FACS plots showed KLRG-1 expression on WT and KO P14 cells on D15 after transfer. **(H)** IFN-γ and TNF production after in vitro stimulation by subsets of WT and KO P14 cells harvested from spleen on D15 after transfer. Graphs showing the frequencies of IFN-γ–producing and TNF- and IFN-γ–producing cells among different subsets of WT and KO P14 cells. Paired Student's t test; *, P < 0.05; **, P < 0.01; ***, P < 0.001; ****, P < 0.0001. **(I)** A summary of GSEA enrichments of WT and KO P14 cells for gene signatures of indicated cell types. Visualized by NES and $-\log_{10}$ (FDR q value). Flow cytometry data in E, G, and H are representative of two independent experiments (n = 4–5 per experiment). RNA-seq datasets were generated from four biological replicates.
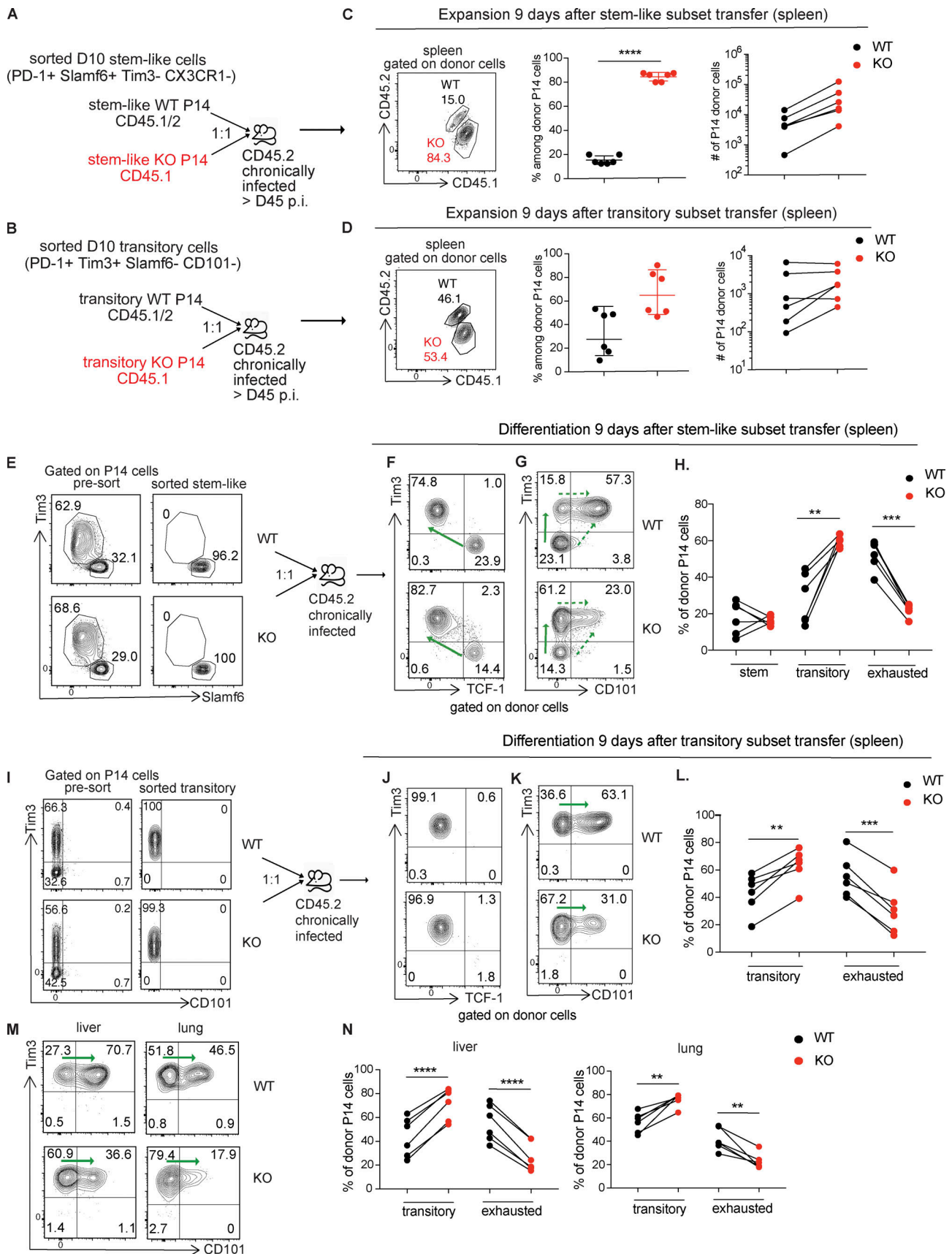
Figure 8. Adoptive transfer of stem-like and transitory subsets into chronically infected mice. (A and B) CD45.1 WT P14 cells or CD45.1.2 KO P14 cells were transferred into CD45.2 naive B6 mice with CD4 T cell depletion, followed by LCMV clone 13 infection. On D10 p.i., Slamf6+ Tim3− CX3CR1− stem-like cells

and Tim3⁺ Slamf6⁻ CD101⁻ transitory cells were sorted from WT and KO P14 donor populations. Mice chronically infected with LCMV (>D45 p.i.) received cotransfer of stem-like WT and KO P14 cells (1:1, 2 × 10⁵ each; A) or transitory WT and KO P14 cells (1:1, 3.5 × 10⁵ each; B). The donor cells were examined on D9 after transfer. **(C and D)** Frequencies and numbers of WT and KO P14 cells in the spleen of mice receiving stem-like WT and KO P14 cells transfer (C) or receiving transitory WT and KO P14 cells transfer (D). Paired Student's t test; ****, $P < 0.0001$. **(E)** FACS plots showing the expression of Tim3 and Slamf6 before and after sorting for stem-like cells on D10 p.i. **(F)** Representative FACS plots showing the expression of Tim3 and TCF-1 by WT and KO P14 cells at 9 d after transfer from the spleen of mice receiving the stem-like WT and KO P14 cells. Solid green arrow showing the differentiation trajectory from stem-like subset to Tim3⁺ differentiated cells. **(G)** Representative FACS plots showing the expression of Tim3 and CD101 by WT and KO P14 cells 9 d after transfer from the spleen of mice receiving the stem-like WT and KO P14 cells. Solid green arrow shows the differentiation trajectory from stem-like cells to transitory cells, and dashed green arrow shows that exhausted cells could emerge from the transitory population or from the stem-like cells. **(H)** Graph showing the frequencies of stem-like (TCF-1⁺ Tim3⁻), transitory (Tim3⁺ CD101⁻), and exhausted (Tim3⁺ CD101⁺) cells generated in the spleen from transferred stem-like WT and KO P14 cells. Paired Student's t test; **, $P < 0.01$; ***, $P < 0.001$. **(I)** FACS plots showing the expression of Tim3 and CD101 before and after sorting for transitory cells on D10 p.i. **(J and K)** Representative FACS plots showing the expression of Tim3 and TCF-1 (J) or Tim3 and CD101 (K) by WT and KO P14 cells in the spleen of mice receiving the transitory WT and KO P14 cells transfer. Solid green arrow shows the differentiation trajectory from transitory cells to exhausted cells. **(L)** Graph showing the frequencies of transitory (Tim3⁺ CD101⁻) and exhausted (Tim3⁺ CD101⁺) WT and KO P14 cells in the spleen of mice receiving the transitory cells transfer. Paired Student's t test; **, $P < 0.01$; ***, $P < 0.001$. **(M)** Representative FACS plot showing the expression of Tim3 and CD101 by WT and KO P14 cells generated from transferred transitory WT and KO P14 cells in the liver and lungs. **(N)** Graph showing the frequencies of transitory (Tim3⁺ CD101⁻) and exhausted (Tim3⁺ CD101⁺) cells among WT and KO P14 cells in the liver and lungs of mice receiving the transitory cells transfer. Paired Student's t test; **, $P < 0.01$; ***, $P < 0.001$ and ****, $P < 0.0001$. Data in B–N are representative of two independent experiments with three mice per experiment. In C, D, H, L, and N, pooled results from two independent experiments (n = 6 total) are shown.

---

subsets (stem, transitory effector, and exhausted) during the course of chronic LCMV infection. Both the transitory effector cells and the stem-like CD8 T cells originate from naive CD8 T cells and are generated during the first week of infection. At this time, the effector CD8 T cells are the dominant population, comprising ∼80% of the P14 cells, and the stem-like subset is ∼15–20%. The more exhausted CD8 T cells are not detectable at this time and start appearing around the second week. As the chronic infection progresses and the milieu becomes more suppressive, the numbers of transitory effector CD8 T cells decline and the numbers of exhausted CD8 T cells increase. This is the typical pattern with WT P14 CD8 T cells. A different pattern is seen with the TGF-βRII KO P14 cells. The most striking difference between WT and KO P14 CD8 T cells is the increased expansion and durability of the transitory effector population in the absence of TGF-β signaling. It should be noted that in these experiments, both the WT and KO P14 CD8 T cells were cotransferred into the same mouse—hence identical conditions, and truly representing differences due to lack of TGF-β signaling directly on the LCMV-specific P14 CD8 T cells. The extended duration of the effector-like subset in KO P14 cells is likely due to a combination of increased differentiation of stem-like CD8 T cells into transitory effector cells, the increased proliferation of the transitory effector cells, and the slower progression to exhaustion. The stage at which TGF-β regulates the differentiation of antigen-specific CD8 T cells during chronic infection is shown in panel B.

It should be noted that both WT and KO P14 cells formed the three clusters of stem-like, transitory, and exhausted cells by their transcriptional profiles at single-cell level (Figs. 4 and S2). Consistent with our flow cytometry data, analysis on scRNA-seq also showed decreased frequencies of KO P14 cells at stem-like and exhausted state, and increased proportions of them at transitory state. Therefore, these data suggest that the absence of TGF-β signaling did not affect the canonical differentiation pathway from stem to transitionary to exhausted, but altered the rate of transition between these states. Indeed, adoptive transfers of purified stem-like and transitory WT and KO P14 cells confirmed that subsets of WT and KO P14 cells followed the same

differentiation trajectory in chronically infected mice, and that TGF-β signaling promoted the progression from transitory effector cells to exhausted cells (Fig. 8).

CD8 T cell differentiation during chronic infection is governed by a complex transcriptional network regulated by multiple signaling pathways and transcription factors (Hashimoto et al., 2018). While it has been shown that TCF-1, together with Bcl-6 and Foxo1, drive the formation of stem-like subset (Im et al., 2016; Utzschneider et al., 2016; Utzschneider et al., 2018; Wu et al., 2016), it remains to be determined how the stemness of this subset is preserved in the environment of chronic infection with sustained antigen exposure. Here we showed that TGF-βRII deletion significantly enhanced the generation of effector-like transitory subset from stem-like cells. Loss of TGF-β signaling led to dysregulated transcription of stem-like CD8 T cell–specific genes, which suggests the potential role of TGF-β signaling in maintaining the unique transcriptional program that serves to protect this subset from further differentiation. Notably, stem-like KO P14 cells failed to upregulate the transcription of several inhibitory receptors/ligands that were specifically expressed on stem-like subset but were not expressed by the more differentiated and exhausted CD8 T cells. Many of these inhibitory molecules are shown to exert their immunosuppressive roles in a paracrine manner. For examples, CD73, together with CD39, convert extracellular ATP into the immunoregulatory nucleotide adenosine (Regateiro et al., 2013). CD200 does not have intracellular signaling domain but it inhibits the activation and proliferation of other cells, such as antigen-presenting cells, that express the inhibitory receptor CD200R (Eckhardt et al., 2014; Gorczynski, 2012). CD83, secreted as soluble form, suppresses T cell activation via its inhibitory effects on monocytes and dendritic cells (Chen et al., 2011; Eckhardt et al., 2014; Horvatinovich et al., 2017). TGF-β may regulate the interaction between antigen-specific CD8 T cells and the myeloid cells and therefore maintain the stem-like state of the resource cells by upregulating these inhibitory molecules. In the absence of TGF-β signaling, there was also reduced transcription of genes associated with the quiescence of stem-like cells, including *Nrp1*, *P2rx7*, and *Lrig1* (Borges da Silva
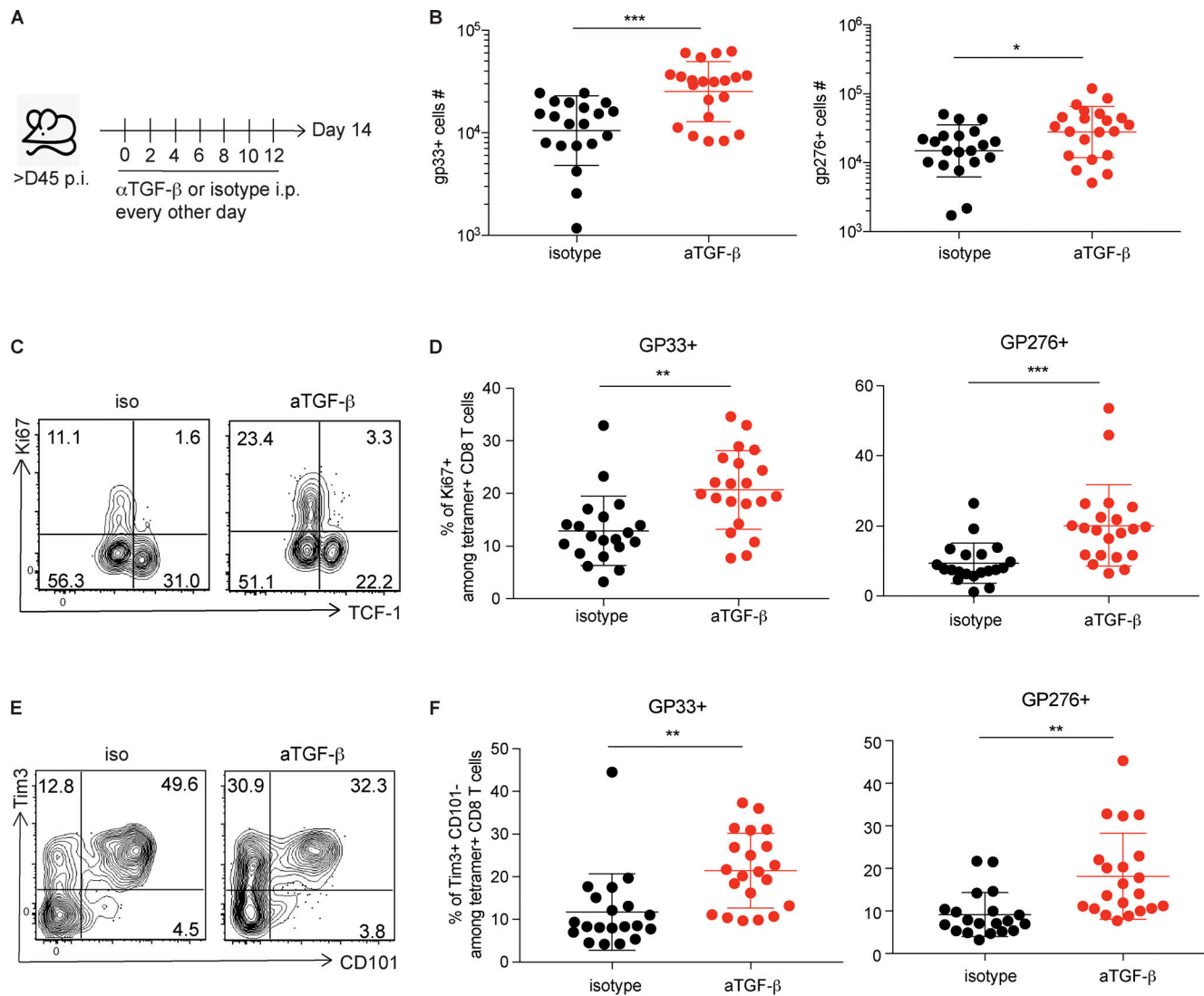
Figure 9. **TGF-β signaling blockade enhances the generation of transitory cells during chronic infection. (A)** Mice chronically infected with LCMV Cl13 (>D45 p.i.) were treated with 1 mg of either anti–TGF-β or isotype control antibodies every other day for 2 wk. **(B)** Numbers of GP33-specific and GP276-specific CD8 T cells in the spleen of chronically infected mice treated with isotype or anti–TGF-β antibodies. Student's *t* test; *, P < 0.05; ***, P < 0.001. **(C)** Representative FACS plots of Ki67 and TCF-1 expression in splenic GP33-specific CD8 T cells. **(D)** Frequencies of Ki67+ cells among GP33-specific and GP276-specific CD8 T cells in the spleen. Student's *t* test; **, P < 0.01; ***, P < 0.001. **(E)** Representative staining of Tim3 and CD101 on GP33-specific CD8 T cells in the spleen. **(F)** Frequencies of transitory Tim3+ CD101– subset among splenic GP33-specific and GP276-specific CD8 T cells. Student's *t* test; **, P < 0.01. Graphs in B, D, and F show the mean and SEM and show pooled data of four independent experiments with five to six mice per experiment.

et al., 2018; Liu et al., 2020; Powell et al., 2012), which may also suggest that the stem-like KO P14 cells are at a more activated state compared with their WT counterpart. In addition, stem cell–like KO P14 cells showed reduced transcription of several transcription factors and signaling molecules that suppress effector properties, including *Tox2*, *Egr1*, *Egr2*, and *Dusp2* (Dan et al., 2020; Seo et al., 2019; Williams et al., 2017). In agreement, a recent study showed that EGR2 was selectively upregulated in stem-like subset during chronic infection and transcriptionally and epigenetically regulated their competency for terminal differentiation (Wagle et al., 2021). *Egr2*, as well as *Egr1* and *Tox2*, is downstream of NFAT signaling, which plays a critical role in programming CD8 T cell exhaustion (Martinez et al., 2015; Seo et al., 2019). Indeed, the transcriptional profile of

stem-like KO P14 cells was negatively enriched with NFAT target genes in exhausted CD8 cells (Martinez et al., 2015). These data suggest that loss of TGF-β signaling disrupts the transcriptional program maintaining the stem-like state in PD-1+ TCF-1+ CD8 T cells and drives them to generate more effector-like transitory cells during chronic infection.

In our studies, we used a model of LCMV clone 13 infection with transient depletion of CD4 T cells that resulted in a lifelong chronic infection with high levels of virus in both lymphoid and nonlymphoid tissues. In this model, CD4 T cells come back to normal within a few weeks, but there is a deficiency of LCMV-specific CD4 T cells (Matloubian et al., 1994). The accompanying manuscript by Ma et al. (2022) in this issue shows that TGF-β is also critical for maintenance of stem-like CD8 T cells during

Figure 10. **The role of TGF-β in CD8 T cell differentiation during chronic infection. (A)** The frequencies of stem-like, transitory, and exhausted subsets among WT and KO P14 cells through LCMV clone 13 infection. **(B)** Model of how TGF-β regulates CD8 T cell differentiation during chronic infection. By inhibiting the effector-associated program, on one hand, TGF-β maintains the quiescence of stem-like subsets and inhibits their differentiation to transitory cells; on the other hand, TGF-β inhibits the proliferation of the transitory cells and promotes their terminal differentiation to exhausted cells.

clone 13 infection with CD4 T cell help. Ma et al. (2022) found that TGF-β maintained stem-like CD8 T cells by regulating the expression of α4 integrins and enforcing their lymphoid retention. In addition, a recent study showed that inhibition of mTOR activity by TGF-β preserved mitochondrial fitness in virus-specific CD8 cells during chronic infection (Gabriel et al., 2021). We also found that loss of TGF-β signaling resulted in significantly enhanced transcription of genes associated with mTOR signaling and glycolysis in P14 cells activated in chronically infected mice. Consistent with the important role of TGF-β in regulating stem-like subset, studies showed that there was increased accessibility of SMAD motif in both mouse and human stem-like CD8 T cells compared with more differentiated cells during chronic infection and cancer (Gabriel et al., 2021; Galletti et al., 2020).

A previous study showed that P14 cells primed in established chronic LCMV infection proliferated and differentiated less under this condition (Snell et al., 2018). Our study now shows that TGF-β is one important player contributing to the reduced expansion and differentiation of P14 cells primed in such an immunosuppressive environment, but other factors, such as antigen presentation and innate immunity, may also play roles

in this setting. An increased concentration of TGF-β1 in the spleen was found at late stage of chronic LCMV infection compared with an earlier time point (Tinoco et al., 2009). In addition, TCR signaling modulates T cell responsiveness to TGF-β by downregulating TGF-βRI. While TGF-β itself can prevent TCR-induced downregulation of TGF-β receptor, this was abrogated by the presence of inflammatory cytokine IL-6 (Tu et al., 2018). Therefore, it is possible that antigen-specific CD8 T cells are more sensitive to the regulation of TGF-β signaling at later stages of chronic infection owing to increased TGF-β concentration in the environment, as well as reduced intensity of TCR signaling and inflammation.

There are also high concentrations of TGF-β in the microenvironment of many types of tumors, and this is linked to poor prognosis (Lin and Zhao, 2015). Recent studies have shown that TGF-β blockade potentiates the effects of PD-1/PD-L1 immune checkpoint therapy by altering peritumoral stroma and increasing T cell infiltration into tumors (Mariathasan et al., 2018; Tauriello et al., 2018). A more recent study examined the feasibility and safety of TGF-β–resistant chimeric antigen receptor T cells in a phase 1 trial and found increased expansion in blood and tumor trafficking of these cells (Narayan et al., 2022). Our

studies now show that TGF-β signaling can also have direct effects on CD8 T cell differentiation during chronic viral infection, and the absence of TGF-β signaling specifically enhanced the accumulation of functional, proliferating, and migratory transitory virus-specific CD8 T cells. These findings have implications for developing better immunotherapies against cancer and chronic viral infections.

Materials and methods

Mice and viral infection

C57BL/6 mice and Rosa26Cre-ERT2 mice were purchased from the Jackson Laboratory. The dLck-Cre TGFβRII$^{flox/flox}$ (KO) mice, generously given by N. Zhang (University of Texas at San Antonio, San Antonio, TX), were crossed to LCMV D^{b}GP33-specific TCR transgenic P14 mice in-house. To induce persistent LCMV infection, 6–8-wk-old female C57BL/6 mice were given anti-CD4–depleting antibody GK1.5 (Bio X Cell) i.p. twice before i.v. infection with 2×10^6 PFU LCMV clone 13 strain (Matloubian et al., 1994). All animal experiments were performed in accordance with the Emory University Institutional Animal Care and Use Committee.

Adoptive transfer and conditional deletion

CD44^{lo} naive CD8 T cells were sorted on a FACS Aria II (BD Biosciences) from dLck-Cre$^+$ TGFβRII$^{flox/flox}$ (KO) and dLck-Cre$^-$ TGFβRII$^{flox/flox}$ (WT) P14 littermate female mice expressing distinct congenic markers. After sorting, congenically marked KO and WT P14 cells were cotransferred into naive C57BL/6 female mice with CD4 T cells depleted 1 d before LCMV clone 13 infection (1:1 ratio, 2×10^3 cells each), or into mice that had been infected 45–60 d earlier with clone 13 (1:1 ratio, 1×10^4 cells each).

For adoptive transfer of stem-like and transitory WT and KO P14 cells, congenically marked WT P14 cells or KO P14 cells were transferred into CD45.2 naive B6 mice with CD4 T cell depletion, followed by LCMV clone 13 infection. On D10 p.i., Slamf6$^+$ Tim3$^-$ CX3CR1$^-$ stem-like cells and Tim3$^+$ Slamf6$^-$ CD101$^-$ transitory cells were sorted from WT and KO P14 donor populations. Stem-like WT and KO P14 cells (1:1 ratio, 1.25×10^5 to 2×10^5 cells each), or transitory WT and KO P14 cells (1:1 ratio, 3.5×10^5 cells each) were cotransferred into the same recipient mice chronically infected with LCMV clone 13 (after D45 p.i.). The donor cells were examined on D9 after transfer.

For conditional deletion of TGF-βRII, naive CD8 T cells from Rosa26Cre-ERT2$^+$ TGF-βRII$^{flox/flox}$ (ER-Cre$^+$ Tgfbr2$^{fl/fl}$) and Rosa26Cre-ERT2$^+$ TGF-βRII$^{+/+}$ (ER-Cre$^+$ WT) P14 littermate female mice were cotransferred into naive B6 mice with CD4 T cells depleted (1:1 ratio, 2×10^3 cells each) 1 d before the recipient mice were infected with LCMV clone 13. On D31 p.i., recipient mice were treated with 1 mg TAM i.p. for 5 consecutive days to induce the deletion of TGF-βRII or with vehicle (sunflower oil) i.p. as controls. ER-Cre$^+$ Tgfbr2$^{fl/fl}$ and ER-Cre$^+$ WT P14 cells (1:1 ratio, 1×10^4 cells each) were also cotransferred into mice chronically infected with LCMV clone 13. Recipient mice were treated with TAM or vehicle for 5 consecutive days (day 0 to day 4 after transfer) to induce the deletion of TGF-βRII.

Flow cytometry

Lymphocytes were harvested from tissues including spleen, blood, liver, and lungs and were strained by fluorochrome-conjugated antibodies directly ex vivo as previously described (Wherry et al., 2003). Antibodies used for flow cytometry were purchased from BD Bioscience, Invitrogen, BioLegend, R&D Systems, and Cell Signaling Technology, including CD8α(53-6.7), CD4(GK1.5), CD19(6D5), CD45.1(104), CD45.2(A20), PD-1(29F.1A12), CD44(IM7), Tim3 (RMT3-23), CXCR5(L138D7), Slamf6(13G3), CD101(Moushi101), CD73(TY/11.8), CD200(OX-90), NRP-1(3E12), P2RX7(1F11), CD200R(OX-110), CX3CR1(SA011F11), IL-18Rα(A17071D), KLRG-1(2F1), IFN-γ(XMG1.2), TNF(MP6-XT22), TCF-1(C63D9), Ki67(B56), EGR2(erongr2), and phospho-S6 ribosomal protein (D57.2.2E).

Briefly, the Foxp3 staining buffer set (Invitrogen) was used for intracellular staining of transcription factors. For intracellular cytokine staining, lymphocytes from spleen were incubated with gp33 peptide in the presence of GolgiPlug and GolgiStop (BD Bioscience) for 5 h at 37°C and analyzed with Cytofix/Cytoperm Kit (BD Bioscience). Phospho-flow was performed directly ex vivo: spleens were harvested at indicated time points, fixed in 2% paraformaldehyde, and permeabilized with BD Phosflow perm buffer III. Data were acquired on a FACS LSR II (BD Biosciences) and an Aurora 5-laser spectral cytometer (Cytek) and analyzed with FlowJo software (TreeStar).

Confocal imaging and histocytometry

KO or WT CD45.1 P14 cells were transferred into separate chronically infected recipient mice (D45 p.i.), and spleens were harvested on D20 after transfer. Immediately after harvesting, spleens were fixed in 1% paraformaldehyde, dehydrated in 30% sucrose, and embedded in optimal cutting temperature (OCT) freezing medium. Subsequently, 15-μm sections were prepared and stained overnight at 4°C. The following antibodies were used: B220 (clone RA3-6B2), CD8a (53-6.7), CD45.1 (A20), F4/80 (BM8), and TCF1 (C63D9). Multicolor confocal images were acquired on a Zeiss 780 tiling microscope equipped with a 40×/1.4-NA oil objective. Image voxels were $0.259 \times 0.259 \times 1$ μm in size. The resulting images were corrected for fluorophore spillover in ImageJ and imported into Imaris software for image processing and cellular segmentation. P14 cells were segmented on the basis of CD45.1 signal using the Imaris built-in surface creation module. Regions comprising B cell follicles, T cell areas, and red pulp were defined based on the expression of B220, CD8, and F4/80, respectively. These positional gates were applied to P14 objects to assess their relative distribution across the different splenic compartments within FlowJo.

RNA-seq

Congenically marked WT and KO P14 cells were adoptively cotransferred into recipient mice as described above. At indicated time points, splenocytes from 6–10 spleens were pooled for each replicate. Donor cells were positively enriched by biotinylated anti-CD45.1 antibody (BioLegend) and anti-biotin Microbeads (Miltenyi Biotec). The enriched cells were stained ex vivo with antibodies against CD45.1, CD45.2, CD8, PD-1, Tim3, and CXCR5 and sorted on a FACSAria II (purity >95%). RNA was extracted

Hu et al.
TGF-β regulates CTLs during chronic infection

Journal of Experimental Medicine   18 of 21
https://doi.org/10.1084/jem.20211574

from sorted cells using an RNAeasy Micro Kit according to the manufacturer's protocol (Qiagen).

Extracted RNA were sent to Emory Yerkes Nonhuman Primate Genomics Core for mRNA library preparation, quality control test, library quantification, and sequencing. FastQ files of reads were aligned to the mouse genome via HISAT2 and FeatureCounts. DESeq2 was used for normalized expression and differential expression analysis. A gene was considered significantly differentially expressed with normalized count of >50, $\log_2$ fold-change >0.6 or <−0.6 (~1.5 fold), and adjusted P value <0.05. For GSEA, genes were preranked by $-\log_{10}$ (adjusted P value) × ($\log_2$[fold-change]). The gene sets used in GSEA include gene signatures associated with CXCR5$^+$ Tim3$^-$ stem-like cells (Im et al., 2016), Tim3$^+$ CD101$^-$ transitory cells, Tim3$^+$ CD101$^+$ terminally exhausted cells (Hudson et al., 2019), circulating gene core, residency gene core (Milner et al., 2017), NFAT target genes in exhausted CD8 T cells (Martinez et al., 2015), and gene signature of IL-7R^{lo} effector cells (Joshi et al., 2007). Enrichments were considered significant with normalized false discovery rate (FDR) <0.05 and were visualized using the corrplot package in R program using normalized enrichment score (NES) and $-\log_{10}$(FDR) (for visualization, since there were enrichments with FDR = 0.0, FDRs were normalized based on a minimal value of 0.001).

scRNA-seq
Congenically marked WT and KO P14 cells were adoptively cotransferred into recipient mice as described above. Donor cells were sorted from the spleen of the recipient mice on D30 p.i. for scRNA-seq. Alignment, filtering, barcode counting, and unique molecular identifier counting were performed using Cell Ranger v3.1. Data were further analyzed using Seurat v.3.1.4. All single-cell analysis was performed using R v.3.6.2. Briefly, cells with a percentage of mitochondrial genes <5% were included. Cells with >3,000 or <1,000 detected genes were considered to be outliers and excluded from the downstream analyses. Principal component analysis was performed, and the six to eight most statistically significant principal components were used for UMAP analysis. Components enriched for cell cycle genes were excluded from UMAP clustering. Marker genes that were differentially expressed within each cluster were identified by the Seurat function FindAllMarkers, with average log fold-change cutoffs of 0.25. Gene set scoring was performed using the VISION R package v.2.1.0, following the scoring algorithm previously described (DeTomaso and Yosef, 2016), and gene sets were generated from data presented in Hudson et al. (2019).

TGF-β blockade experiment
C57BL/6J mice were infected with LCMV clone 13 as described above. On >45 d p.i., mice were injected with 1 mg of anti–TGF-β antibody (clone 1D11.16.8; Bio X Cell) or isotype control (mouse IgG1κ; Bio X Cell) every other day for 2 wk. Mice were analyzed for antigen-specific CD8 T cell response 2 d after the last treatment.

Online supplemental material
Fig. S1 shows the phenotype and effector function of WT and TGF-βRII KO P14 CD8 T cells during chronic LCMV infection. Fig. S2 shows the scRNA-seq analysis of WT and KO P14 cells on D30 p.i. Fig. S3 shows the expansion of WT vs. KO P14 cells in two different settings (activated at the onset of infection vs. activated in established chronic infection), proliferation of WT vs. KO P14 cells in chronically infected mice, and phenotypes resulting from the conditional deletion of TGF-βRII on P14 cells activated in established chronic infection. Fig. S4 shows the anatomic location of WT vs. KO P14 cells in the spleen of chronically infected mice on D20 after transfer. Fig. S5 shows the relative expression of selected genes in WT vs. KO P14 cells harvested on D12 after transfer into chronically infected mice. Table S1 lists genes significantly differentially expressed in D15 and D30 Tim3$^+$ WT vs. KO P14 cells, and in D8, D15, and D30 CXCR5$^+$ WT vs. KO P14 cells. Table S2 lists genes significantly differentially expressed in WT vs. KO P14 cells on D12 after transfer into chronically infected mice.

Data availability
Data from RNA-seq of Tim3$^+$-differentiated and CXCR5$^+$ stem-like WT vs. TGFβRII KO P14 cells (Fig. 2 and Fig. 3) are available in the Gene Expression Omnibus (GEO) database under accession no. GSE209598 (D8 and D15 after LCMV clone 13 infection) and no. GSE209590 (D30 p.i.). Data from RNA-seq of WT vs. TGFβRII KO P14 cells transferred into chronically infected mice (Fig. 7) are available in the GEO database under accession no. GSE209577. Data from scRNA-seq of WT vs. TGFβRII KO P14 cells at D30 p.i. (Fig. 4) are available in the GEO database under accession no. GSE210157.

PD-1 issued and a patent for inhibitory molecules specifically expressed by a subset of stem-like CD8 T cells for therapeutic intervention pending. No other disclosures were reported.

References

Alfei, F., K. Kanev, M. Hofmann, M. Wu, H.E. Ghoneim, P. Roelli, D.T. Utzschneider, M.von Hoesslin, J.G. Cullen, Y. Fan, et al. 2019. TOX reinforces the phenotype and longevity of exhausted T cells in chronic viral infection. *Nature* 571:265–269. https://doi.org/10.1038/s41586-019-1326-9

Barber, D.L., E.J. Wherry, D. Masopust, B. Zhu, J.P. Allison, A.H. Sharpe, G.J. Freeman, and R. Ahmed. 2006. Restoring function in exhausted CD8 T cells during chronic viral infection. *Nature*. 439:682–687. https://doi.org/10.1038/nature04444

Batlle, E., and J. Massagué. 2019. Transforming growth factor-β signaling in immunity and cancer. *Immunity*. 50:924–940. https://doi.org/10.1016/j.immuni.2019.03.024

Boettler, T., Y. Cheng, K. Ehrhardt, and M. von Herrath. 2012. TGF-β blockade does not improve control of an established persistent viral infection. *Viral Immunol.* 25:232–238. https://doi.org/10.1089/vim.2011.0079

Borges da Silva, H., L.K. Beura, H. Wang, E.A. Hanse, R. Gore, M.C. Scott, D.A. Walsh, K.E. Block, R. Fonseca, Y. Yan, et al. 2018. The purinergic receptor P2RX7 directs metabolic fitness of long-lived memory CD8+ T cells. *Nature*. 559:264–268. https://doi.org/10.1038/s41586-018-0282-0

Brahmer, J.R., S.S. Tykodi, L.Q.M. Chow, W.-J. Hwu, S.L. Topalian, P. Hwu, C.G. Drake, L.H. Camacho, J. Kauh, K. Odunsi, et al. 2012. Safety and activity of anti–PD-L1 antibody in patients with advanced cancer. *N. Engl. J. Med.* 366:2455–2465. https://doi.org/10.1056/NEJMoa1200694

Brummelman, J., E.M.C. Mazza, G. Alvisi, F.S. Colombo, A. Grilli, J. Mikulak, D. Mavilio, M. Alloisio, F. Ferrari, E. Lopci, et al. 2018. High-dimensional single cell analysis identifies stem-like cytotoxic CD8+ T cells infiltrating human tumors. *J. Exp. Med.* 215:2520–2535. https://doi.org/10.1084/jem.20180684

Carlson, C.M., B.T. Endrizzi, J. Wu, X. Ding, M.A. Weinreich, E.R. Walsh, M.A. Wani, J.B. Lingrel, K.A. Hogquist, and S.C. Jameson. 2006. Kruppel-like factor 2 regulates thymocyte and T-cell migration. *Nature*. 442:299–302. https://doi.org/10.1038/nature04882

Chen, L., Y. Zhu, G. Zhang, C. Gao, W. Zhong, and X. Zhang. 2011. CD83-stimulated monocytes suppress T-cell immune responses through production of prostaglandin E2. *Proc. Natl. Acad. Sci. USA.* 108:18778–18783. https://doi.org/10.1073/pnas.1018994108

Collins, S., M.A. Lutz, P.E. Zarek, R.A. Anders, G.J. Kersh, and J.D. Powell. 2008. Opposing regulation of T cell function by Egr-1/NAB2 and Egr-2/Egr-3. *Eur. J. Immunol.* 38:528–536. https://doi.org/10.1002/eji.200737157

Dan, L., L. Liu, Y. Sun, J. Song, Q. Yin, G. Zhang, F. Qi, Z. Hu, Z. Yang, Z. Zhou, et al. 2020. The phosphatase PAC1 acts as a T cell suppressor and attenuates host antitumor immunity. *Nat. Immunol.* 21:287–297. https://doi.org/10.1038/s41590-019-0577-9

Day, C.L., D.E. Kaufmann, P. Kiepiela, J.A. Brown, E.S. Moodley, S. Reddy, E.W. Mackey, J.D. Miller, A.J. Leslie, C. DePierres, et al. 2006. PD-1 expression on HIV-specific T cells is associated with T-cell exhaustion and disease progression. *Nature*. 443:350–354. https://doi.org/10.1038/nature05115

DeTomaso, D., and N. Yosef. 2016. FastProject: A tool for low-dimensional analysis of single-cell RNA-seq data. *BMC Bioinformatics*. 17:315. https://doi.org/10.1186/s12859-016-1176-5

Eckhardt, J., S. Kreiser, M. Döbbeler, C. Nicolette, M.A. DeBenedette, I.Y. Tcherepanova, C. Ostalecki, A.J. Pommer, C. Becker, C. Günther, et al. 2014. Soluble CD83 ameliorates experimental colitis in mice. *Mucosal Immunol.* 7:1006–1018. https://doi.org/10.1038/mi.2013.119

Gabriel, S.S., C. Tsui, D. Chisanga, F. Weber, M. Llano-León, P.M. Gubser, L. Bartholin, F. Souza-Fonseca-Guimaraes, N.D. Huntington, W. Shi, et al. 2021. Transforming growth factor-β-regulated mTOR activity preserves cellular metabolism to maintain long-term T cell responses in chronic infection. *Immunity*. 54:1698–1714.e5. https://doi.org/10.1016/j.immuni.2021.06.007

Galletti, G., G. De Simone, E.M.C. Mazza, S. Puccio, C. Mezzanotte, T.M. Bi, A.N. Davydov, M. Metsger, E. Scamardella, G. Alvisi, et al. 2020. Two subsets of stem-like CD8+ memory T cell progenitors with distinct fate commitments in humans. *Nat. Immunol.* 21:1552–1562. https://doi.org/10.1038/s41590-020-0791-5

Gallimore, A., A. Glithero, A. Godkin, A.C. Tissot, A. Plückthun, T. Elliott, H. Hengartner, and R. Zinkernagel. 1998. Induction and exhaustion of lymphocytic choriomeningitis virus–specific cytotoxic T lymphocytes visualized using soluble tetrameric major histocompatibility complex class I–peptide complexes. *J. Exp. Med.* 187:1383–1393. https://doi.org/10.1084/jem.187.9.1383

Garidou, L., S. Heydari, S. Gossa, and D.B. McGavern. 2012. Therapeutic blockade of transforming growth factor beta fails to promote clearance of a persistent viral infection. *J. Virol.* 86:7060–7071. https://doi.org/10.1128/JVI.00164-12

Gong, J., A. Chehrazi-Raffle, S. Reddi, and R. Salgia. 2018. Development of PD-1 and PD-L1 inhibitors as a form of cancer immunotherapy: A comprehensive review of registration trials and future considerations. *J. Immunother. Cancer.* 6:8. https://doi.org/10.1186/s40425-018-0316-z

Gorczynski, R.M. 2012. CD200:CD200R-Mediated regulation of immunity. *ISRN Immunol.* 2012. https://doi.org/10.5402/2012/682168

Hashimoto, M., A.O. Kamphorst, S.J. Im, H.T. Kissick, R.N. Pillai, S.S. Ramalingam, K. Araki, and R. Ahmed. 2018. CD8 T cell exhaustion in chronic infection and cancer: Opportunities for interventions. *Annu. Rev. Med.* 69:301–318. https://doi.org/10.1146/annurev-med-012017-043208

He, R., S. Hou, C. Liu, A. Zhang, Q. Bai, M. Han, Y. Yang, G. Wei, T. Shen, X. Yang, et al. 2016. Follicular CXCR5-expressing CD8+ T cells curtail chronic viral infection. *Nature*. 537:412–428. https://doi.org/10.1038/nature19317

Horvatinovich, J.M., E.W. Grogan, M. Norris, A. Steinkasserer, H. Lemos, A.L. Mellor, I.Y. Tcherepanova, C.A. Nicolette, and M.A. DeBenedette. 2017. Soluble CD83 inhibits T cell activation by binding to the TLR4/MD-2 complex on CD14(+) monocytes. *J. Immunol.* 198:2286–2301. https://doi.org/10.4049/jimmunol.1600802

Hudson, W.H., J. Gensheimer, M. Hashimoto, A. Wieland, R.M. Valanparambil, P. Li, J.-X. Lin, B.T. Konieczny, S.J. Im, G.J. Freeman, et al. 2019. Proliferating transitory T cells with an effector-like transcriptional signature emerge from PD-1+ stem-like CD8+ T cells during chronic infection. *Immunity*. 51:1043–1058.e4. https://doi.org/10.1016/j.immuni.2019.11.002

Im, S.J., M. Hashimoto, M.Y. Gerner, J. Lee, H.T. Kissick, M.C. Burger, Q. Shan, J.S. Hale, J. Lee, T.H. Nasti, et al. 2016. Defining CD8+ T cells that provide the proliferative burst after PD-1 therapy. *Nature*. 537:417–421. https://doi.org/10.1038/nature19330

Im, S.J., B.T. Konieczny, W.H. Hudson, D. Masopust, and R. Ahmed. 2020. PD-1+ stemlike CD8 T cells are resident in lymphoid tissues during persistent LCMV infection. *Proc. Natl. Acad. Sci. USA.* 117:4292–4299. https://doi.org/10.1073/pnas.1917298117

Jadhav, R.R., S.J. Im, B. Hu, M. Hashimoto, P. Li, J.-X. Lin, W.J. Leonard, W.J. Greenleaf, R. Ahmed, and J.J. Goronzy. 2019. Epigenetic signature of PD-1+ TCF1+ CD8 T cells that act as resource cells during chronic viral infection and respond to PD-1 blockade. *Proc. Natl. Acad. Sci. USA.* 116:14113–14118. https://doi.org/10.1073/pnas.1903520116

Jenne, C.N., A. Enders, R. Rivera, S.R. Watson, A.J. Bankovich, J.P. Pereira, Y. Xu, C.M. Roots, J.N. Beilke, A. Banerjee, et al. 2009. T-bet–dependent S1P5 expression in NK cells promotes egress from lymph nodes and bone marrow. *J. Exp. Med.* 206:2469–2481. https://doi.org/10.1084/jem.20090525

Joshi, N.S., W. Cui, A. Chandele, H.K. Lee, D.R. Urso, J. Hagman, L. Gapin, and S.M. Kaech. 2007. Inflammation directs memory precursor and short-lived effector CD8+ T cell fates via the graded expression of T-bet transcription factor. *Immunity*. 27:281–295. https://doi.org/10.1016/j.immuni.2007.07.010

Khan, O., J.R. Giles, S. McDonald, S. Manne, S.F. Ngiow, K.P. Patel, M.T. Werner, A.C. Huang, K.A. Alexander, J.E. Wu, et al. 2019. TOX transcriptionally and epigenetically programs CD8+ T cell exhaustion. *Nature*. 571:211–218. https://doi.org/10.1038/s41586-019-1325-x

Lewis, G.M., E.J. Wehrens, L. Labarta-Bajo, H. Streeck, and E.I. Zuniga. 2016. TGF-β receptor maintains CD4 T helper cell identity during chronic viral infections. *J. Clin. Invest.* 126:3799–3813. https://doi.org/10.1172/JCI87041

Lin, R.-L., and L.-J. Zhao. 2015. Mechanistic basis and clinical relevance of the role of transforming growth factor-β in cancer. *Cancer Biol. Med.* 12:385–393. https://doi.org/10.7497/j.issn.2095-3941.2015.0015

Liu, C., A. Somasundaram, S. Manne, A.M. Gocher, A.L. Szymczak-Workman, K.M. Vignali, E.N. Scott, D.P. Normolle, E. John Wherry, E.J. Lipson, et al. 2020. Neuropilin-1 is a T cell memory checkpoint limiting long-

term antitumor immunity. *Nat. Immunol.* 21:1010–1021. https://doi.org/10.1038/s41590-020-0733-2

Ma, C., and N. Zhang. 2015. Transforming growth factor-β signaling is constantly shaping memory T-cell population. *Proc. Natl. Acad. Sci. USA.* 112:11013–11017. https://doi.org/10.1073/pnas.1510119112

Ma, C., L. Wang, W. Liao, Y. Liu, S. Mishra, G. Li, X. Zhang, Y. Qiu, Q. Lu, and N. Zhang. 2022. TGF-β promotes stem-like T cells via enforcing their lymphoid tissue retention. *J. Exp. Med.* 219. https://doi.org/10.1084/jem.20211538

Mariathasan, S., S.J. Turley, D. Nickles, A. Castiglioni, K. Yuen, Y. Wang, E.E. Kadel Iii, H. Koeppen, J.L. Astarita, R. Cubas, et al. 2018. TGFβ attenuates tumour response to PD-L1 blockade by contributing to exclusion of T cells. *Nature.* 554:544–548. https://doi.org/10.1038/nature25501

Martinez, G.J., R.M. Pereira, T. Äijö, E.Y. Kim, F. Marangoni, M.E. Pipkin, S. Togher, V. Heissmeyer, Y.C. Zhang, S. Crotty, et al. 2015. The transcription factor NFAT promotes exhaustion of activated CD8$^+$ T cells. *Immunity.* 42:265–278. https://doi.org/10.1016/j.immuni.2015.01.006

Matloubian, M., R.J. Concepcion, and R. Ahmed. 1994. CD4+ T cells are required to sustain CD8+ cytotoxic T-cell responses during chronic viral infection. *J. Virol.* 68:8056–8063. https://doi.org/10.1128/JVI.68.12.8056-8063.1994

McLane, L.M., M.S. Abdel-Hakeem, and E.J. Wherry. 2019. CD8 T cell exhaustion during chronic viral infection and cancer. *Annu. Rev. Immunol.* 37:457–495. https://doi.org/10.1146/annurev-immunol-041015-055318

Milner, J.J., C. Toma, B. Yu, K. Zhang, K. Omilusik, A.T. Phan, D. Wang, A.J. Getzler, T. Nguyen, S. Crotty, et al. 2017. Runx3 programs CD8+ T cell residency in non-lymphoid tissues and tumours. *Nature.* 552:253–257. https://doi.org/10.1038/nature24993

Narayan, V., J.S. Barber-Rotenberg, I.-Y. Jung, S.F. Lacey, A.J. Rech, M.M. Davis, W.-T. Hwang, P. Lal, E.L. Carpenter, S.L. Maude, et al. 2022. PSMA-Targeting TGFβ-insensitive armored CAR T cells in metastatic castration-resistant prostate cancer: A phase 1 trial. *Nat. Med.* 28:724–734. https://doi.org/10.1038/s41591-022-01726-1

Pircher, H., D. Moskophidis, U. Rohrer, K. Bürki, H. Hengartner, and R.M. Zinkernagel. 1990. Viral escape by selection of cytotoxic T cell-resistant virus variants in vivo. *Nature.* 346:629–633. https://doi.org/10.1038/346629a0

Powell, A.E., Y. Wang, Y. Li, E.J. Poulin, A.L. Means, M.K. Washington, J.N. Higginbotham, A. Juchheim, N. Prasad, S.E. Levy, et al. 2012. The pan-ErbB negative regulator Lrig1 is an intestinal stem cell marker that functions as a tumor suppressor. *Cell.* 149:146–158. https://doi.org/10.1016/j.cell.2012.02.042

Regateiro, F.S., S.P. Cobbold, and H. Waldmann. 2013. CD73 and adenosine generation in the creation of regulatory microenvironments. *Clin. Exp. Immunol.* 171:1–7. https://doi.org/10.1111/j.1365-2249.2012.04623.x

Sanjabi, S., S.A. Oh, and M.O. Li. 2017. Regulation of the immune response by TGF-β: From conception to autoimmunity and infection. *Cold Spring Harb. Perspect. Biol.* 9:a022236. https://doi.org/10.1101/cshperspect.a022236

Schenkel, J.M., and D. Masopust. 2014. Tissue-resident memory T cells. *Immunity.* 41:886–897. https://doi.org/10.1016/j.immuni.2014.12.007

Scott, A.C., F. Dündar, P. Zumbo, S.S. Chandran, C.A. Klebanoff, M. Shakiba, P. Trivedi, L. Menocal, H. Appleby, S. Camara, et al. 2019. TOX is a critical regulator of tumour-specific T cell differentiation. *Nature.* 571:270–274. https://doi.org/10.1038/s41586-019-1324-y

Seo, H., J. Chen, E. González-Avalos, D. Samaniego-Castruita, A. Das, Y.H. Wang, I.F. López-Moyado, R.O. Georges, W. Zhang, A. Onodera, et al. 2019. TOX and TOX2 transcription factors cooperate with NR4A transcription factors to impose CD8+ T cell exhaustion. *Proc. Natl. Acad. Sci. USA.* 116:12410–12415. https://doi.org/10.1073/pnas.1905675116

Shi, Y., and J. Massagué. 2003. Mechanisms of TGF-β signaling from cell membrane to the nucleus. *Cell.* 113:685–700. https://doi.org/10.1016/s0092-8674(03)00432-x

Skon, C.N., J.-Y. Lee, K.G. Anderson, D. Masopust, K.A. Hogquist, and S.C. Jameson. 2013. Transcriptional downregulation of S1pr1 is required for the establishment of resident memory CD8+ T cells. *Nat. Immunol.* 14:1285–1293. https://doi.org/10.1038/ni.2745

Snell, L.M., B.L. MacLeod, J.C. Law, I. Osokine, H.J. Elsaesser, K. Hezaveh, R.J. Dickson, M.A. Gavin, C.J. Guidos, T.L. McGaha, and D.G. Brooks. 2018. CD8+ T cell priming in established chronic viral infection preferentially directs differentiation of memory-like cells for sustained immunity. *Immunity.* 49:678–694.e5. https://doi.org/10.1016/j.immuni.2018.08.002

Tauriello, D.V.F., S. Palomo-Ponce, D. Stork, A. Berenguer-Llergo, J. Badia-Ramentol, M. Iglesias, M. Sevillano, S. Ibiza, A. Cañellas, X. Hernando-Momblona, et al. 2018. TGFβ drives immune evasion in genetically reconstituted colon cancer metastasis. *Nature.* 554:538–543. https://doi.org/10.1038/nature25492

Tinoco, R., V. Alcalde, Y. Yang, K. Sauer, and E.I. Zuniga. 2009. Cell-intrinsic transforming growth factor-β signaling mediates virus-specific CD8+ T cell deletion and viral persistence in vivo. *Immunity.* 31:145–157. https://doi.org/10.1016/j.immuni.2009.06.015

Topalian, S.L., F.S. Hodi, J.R. Brahmer, S.N. Gettinger, D.C. Smith, D.F. McDermott, J.D. Powderly, R.D. Carvajal, J.A. Sosman, M.B. Atkins, et al. 2012. Safety, activity, and immune correlates of anti–PD-1 antibody in cancer. *N. Engl. J. Med.* 366:2443–2454. https://doi.org/10.1056/NEJMoa1200690

Tu, E., C.P.Z. Chia, W. Chen, D. Zhang, S.A. Park, W. Jin, D. Wang, M.-L. Alegre, Y.E. Zhang, L. Sun, and W. Chen. 2018. T cell receptor-regulated TGF-β type I receptor expression determines T cell quiescence and activation. *Immunity.* 48:745–759.e6. https://doi.org/10.1016/j.immuni.2018.03.025

Utzschneider, D.T., M. Charmoy, V. Chennupati, L. Pousse, D.P. Ferreira, S. Calderon-Copete, M. Danilo, F. Alfei, M. Hofmann, D. Wieland, et al. 2016. T cell factor 1-expressing memory-like CD8+ T cells sustain the immune response to chronic viral infections. *Immunity.* 45:415–427. https://doi.org/10.1016/j.immuni.2016.07.021

Utzschneider, D.T., A. Delpoux, D. Wieland, X. Huang, C.-Y. Lai, M. Hofmann, R. Thimme, and S.M. Hedrick. 2018. Active maintenance of T cell memory in acute and chronic viral infection depends on continuous expression of FOXO1. *Cell Rep.* 22:3454–3467. https://doi.org/10.1016/j.celrep.2018.03.020

Vaddepally, R.K., P. Kharel, R. Pandey, R. Garje, and A.B. Chandra. 2020. Review of indications of FDA-approved immune checkpoint inhibitors per NCCN guidelines with the level of evidence. *Cancers.* 12:738. https://doi.org/10.3390/cancers12030738

Wagle, M.V., S.J. Vervoort, M.J. Kelly, W. Van Der Byl, T.J. Peters, B.P. Martin, L.G. Martelotto, S. Nüssing, K.M. Ramsbottom, J.R. Torpy, et al. 2021. Antigen-driven EGR2 expression is required for exhausted CD8+ T cell stability and maintenance. *Nat. Commun.* 12:2782. https://doi.org/10.1038/s41467-021-23044-9

Wherry, E.J., J.N. Blattman, K. Murali-Krishna, R. van der Most, and R. Ahmed. 2003. Viral persistence alters CD8 T-cell immunodominance and tissue distribution and results in distinct stages of functional impairment. *J. Virol.* 77:4911–4927. https://doi.org/10.1128/jvi.77.8.4911-4927.2003

Wherry, E.J., S.-J. Ha, S.M. Kaech, W.N. Haining, S. Sarkar, V. Kalia, S. Subramaniam, J.N. Blattman, D.L. Barber, and R. Ahmed. 2007. Molecular signature of CD8+ T cell exhaustion during chronic viral infection. *Immunity.* 27:670–684. https://doi.org/10.1016/j.immuni.2007.09.006

Williams, J.B., B.L. Horton, Y. Zheng, Y. Duan, J.D. Powell, and T.F. Gajewski. 2017. The EGR2 targets LAG-3 and 4-1BB describe and regulate dysfunctional antigen-specific CD8+ T cells in the tumor microenvironment. *J. Exp. Med.* 214:381–400. https://doi.org/10.1084/jem.20160485

Wu, T., Y. Ji, E.A. Moseman, H.C. Xu, M. Manglani, M. Kirby, S.M. Anderson, R. Handon, E. Kenyon, A. Elkahloun, et al. 2016. The TCF1-Bcl6 axis counteracts type I interferon to repress exhaustion and maintain T cell stemness. *Sci. Immunol.* 1:eaai8593. https://doi.org/10.1126/sciimmunol.aai8593

Zajac, A.J., J.N. Blattman, K. Murali-Krishna, D.J. Sourdive, M. Suresh, J.D. Altman, and R. Ahmed. 1998. Viral immune evasion due to persistence of activated T cells without effector function. *J. Exp. Med.* 188:2205–2213. https://doi.org/10.1084/jem.188.12.2205

Zander, R., D. Schauder, G. Xin, C. Nguyen, X. Wu, A. Zajac, and W. Cui. 2019. CD4+ T cell help is required for the formation of a cytolytic CD8+ T cell subset that protects against chronic infection and cancer. *Immunity.* 51:1028–1042.e4. https://doi.org/10.1016/j.immuni.2019.10.009

Zhang, N., and M.J. Bevan. 2012. TGF-β signaling to T cells inhibits autoimmunity during lymphopenia-driven proliferation. *Nat. Immunol.* 13:667–673. https://doi.org/10.1038/ni.2319

Zhang, N., and M.J. Bevan. 2013. Transforming growth factor-β signaling controls the formation and maintenance of gut-resident memory T cells by regulating migration and retention. *Immunity.* 39:687–696. https://doi.org/10.1016/j.immuni.2013.08.019

Supplemental material
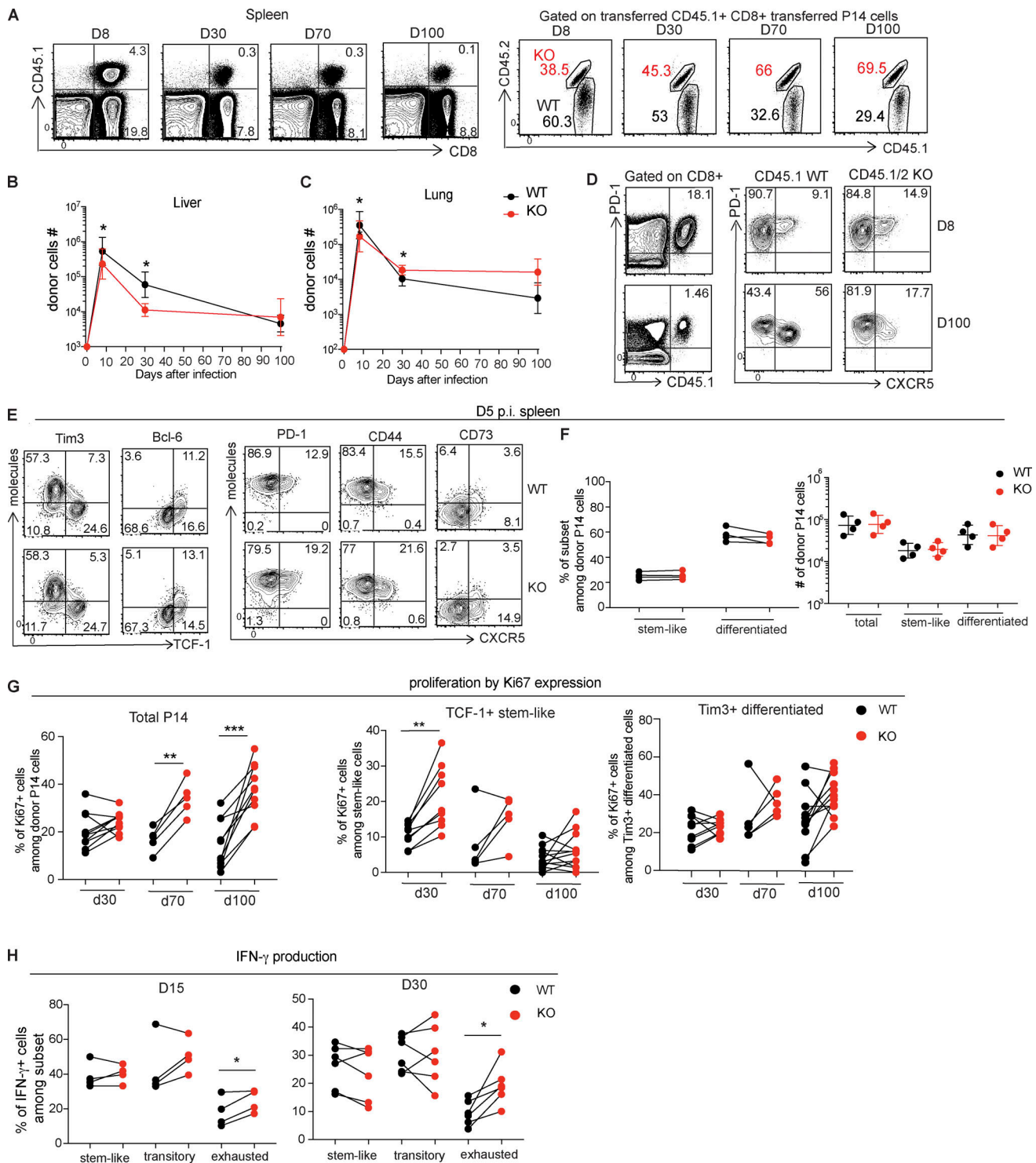
Figure S1. **TGF-β regulates CD8 T cell differentiation during chronic infection.** Congenically marked WT and Tgfbr2−/− (KO) LCMV GP33-specific P14 CD8 T cells were cotransferred into naive mice treated with anti-CD4 depleting antibody GK1.5, followed by LCMV Cl13 infection. **(A)** Representative FACS plots show frequencies of CD45.1+ donor cells in the spleen after Cl13 infection, gated on lymphocytes (left), and the ratio of WT and KO P14 cells in the spleen, gated on donor P14 cells (right). **(B and C)** Longitudinal analysis of the numbers of WT and KO P14 cells in liver (B) and lungs (C). Graph shows the mean and SEM. Paired Student's t test; *, P < 0.05. **(D)** Representative FACS plots show the expression of PD-1 on WT and KO P14 cells in the spleen at indicated time points. **(E)** Phenotype of WT and KO P14 cells in the spleen on D5 p.i. **(F)** Graphs showed the frequencies and numbers of subsets of WT and KO P14 cells on D5 p.i. Data in A–F are representative of three independent experiments (n = 4–6 each time point per experiment). **(G)** Pool results from two independent experiments (n = 4–5 mice per time point per experiment) showing frequencies of Ki67-expressing cells among total WT and KO P14 cells (left), among TCF-1+ Tim3− stem-like WT and KO P14 cells (middle), and among Tim3+ TCF-1− differentiated WT and KO P14 cells (right) at indicated time points. Paired Student's t test; **, P < 0.01; ***, P<0.001. **(H)** Production of IFN-γ by subsets of WT and KO P14 cells harvested from spleen on D15 and D30 after in vitro stimulation with GP33 peptide. Paired Student's t test; *, P < 0.05. Data are representative of two independent experiments (n = 4–6 per time point per experiment).
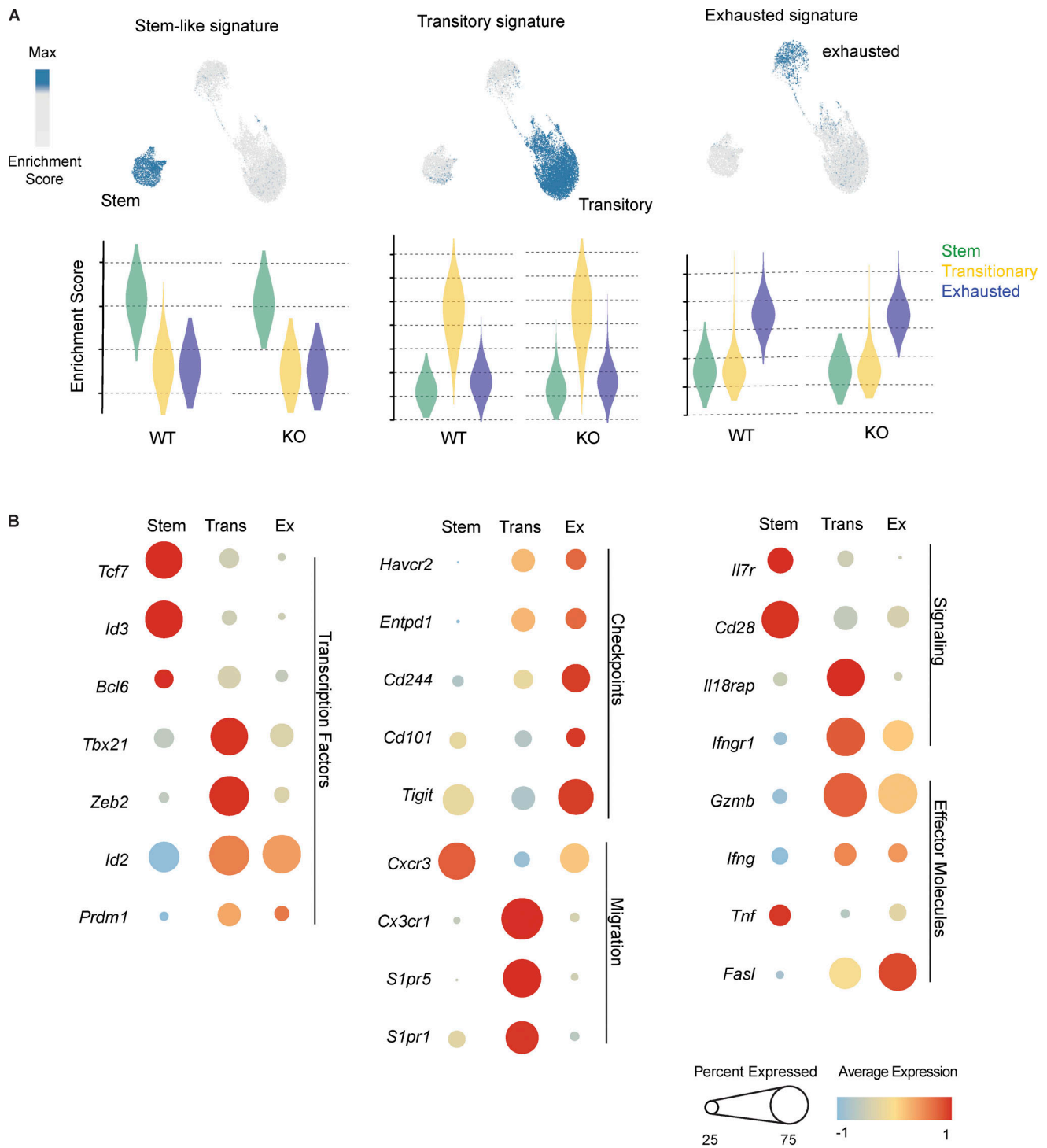
Figure S2. **scRNA-seq of WT and TGF-βRII–deficient P14 cells from chronically infected mice. (A)** VISION analyses of WT and KO P14 cells for enrichment of gene signatures associated with LCMV-specific stem-like, transitory, and exhausted CD8 T cells. UMAP plots identified the cells enriched for each gene signature shown in blue color. Violin plots showed the enrichment of each gene signature in the clusters of WT and KO P14 cells (stem, transitory, and exhausted). **(B)** Dot plots showing the relative expression levels and the percentages of cells in each cluster expressing the selected genes.
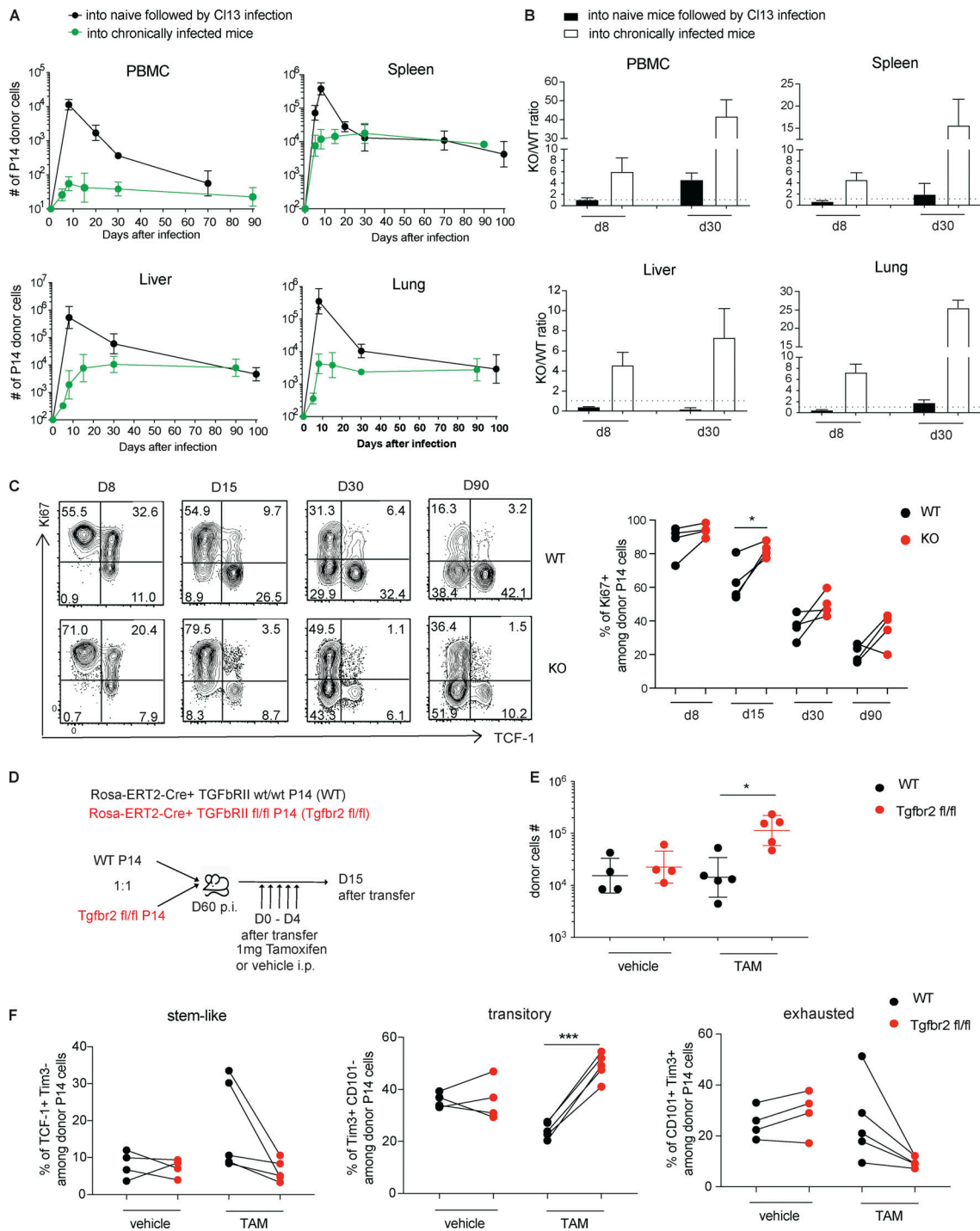
Figure S3. **TGF-β suppresses the expansion and differentiation of antigen-specific CD8 T cells activated in an established chronic infection.** **(A)** Reduced expansion of antigen-specific CD8 T cells activated in the immunosuppressive environment of an established chronic infection. Longitudinal analysis compared the numbers of WT P14 cells when 2×10^3 P14 cells were transfer into naive mice followed by LCMV Clone 13 infection (black) vs. when 1×10^4 P14 cells were into mice with established chronic LCMV infection (>day 45 p.i.; green). **(B)** KO/WT ratio when P14 cells were transferred in a 1:1 ratio into naive mice followed by LCMV Clone 13 infection or into mice with established chronic LCMV infection. Data in A and B are representative of three independent experiments (n = 4–5 each time point per experiment). **(C)** Expression of Ki67 and TCF-1 by WT and KO P14 cells in the spleen at indicated time points after transfer. Paired Student's t test; *, P < 0.05. Data are representative of three independent experiments (n = 4–5 each time point per experiment). **(D)** Rosa26Cre-ERT2+ (ER-Cre+) TGF-βRII^fl/fl (Tgfbr2^fl/fl) and ER-Cre+ TGF-βRII^+/+(WT) P14 cells were cotransferred into mice chronically infected with LCMV clone 13. Recipient mice were treated with TAM or vehicle for 5 consecutive days (day 0–4 after transfer) to induce the deletion of TGF-βRII. Donor cells were harvested from spleen on D15 after transfer. **(E)** Numbers of ER-Cre+ WT and ER-Cre+ Tgfbr2^fl/fl P14 cells in the spleen of mice treated with vehicle or TAM. Paired Student's t test; *, P < 0.05. **(F)** Plots show frequencies of TCF-1+ Tim3− stem-like cells, Tim3+ CD101− transitory cells, and Tim3+ CD101+ exhausted cells among ER-Cre+ WT and ER-Cre+ Tgfbr2^fl/fl P14 cells in the spleen. Paired Student's t test; ***, P < 0.001. Data in E and F are representative of two independent experiments (n = 4–6 each time point per experiment).
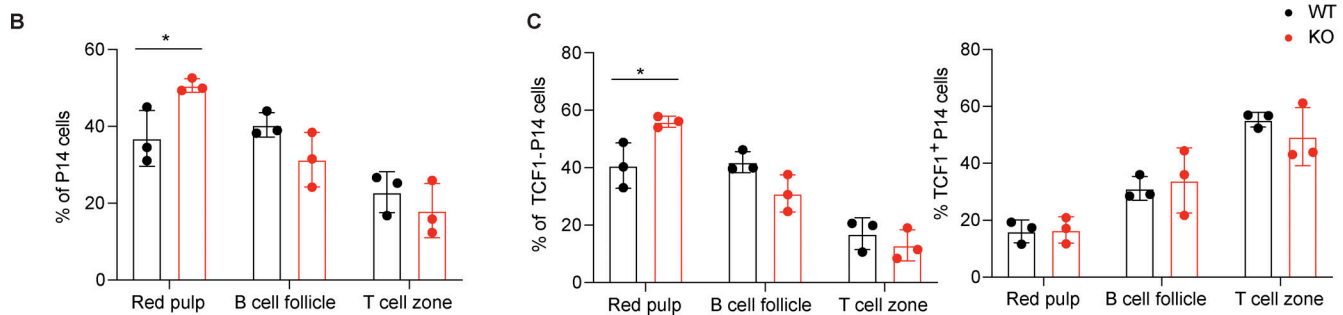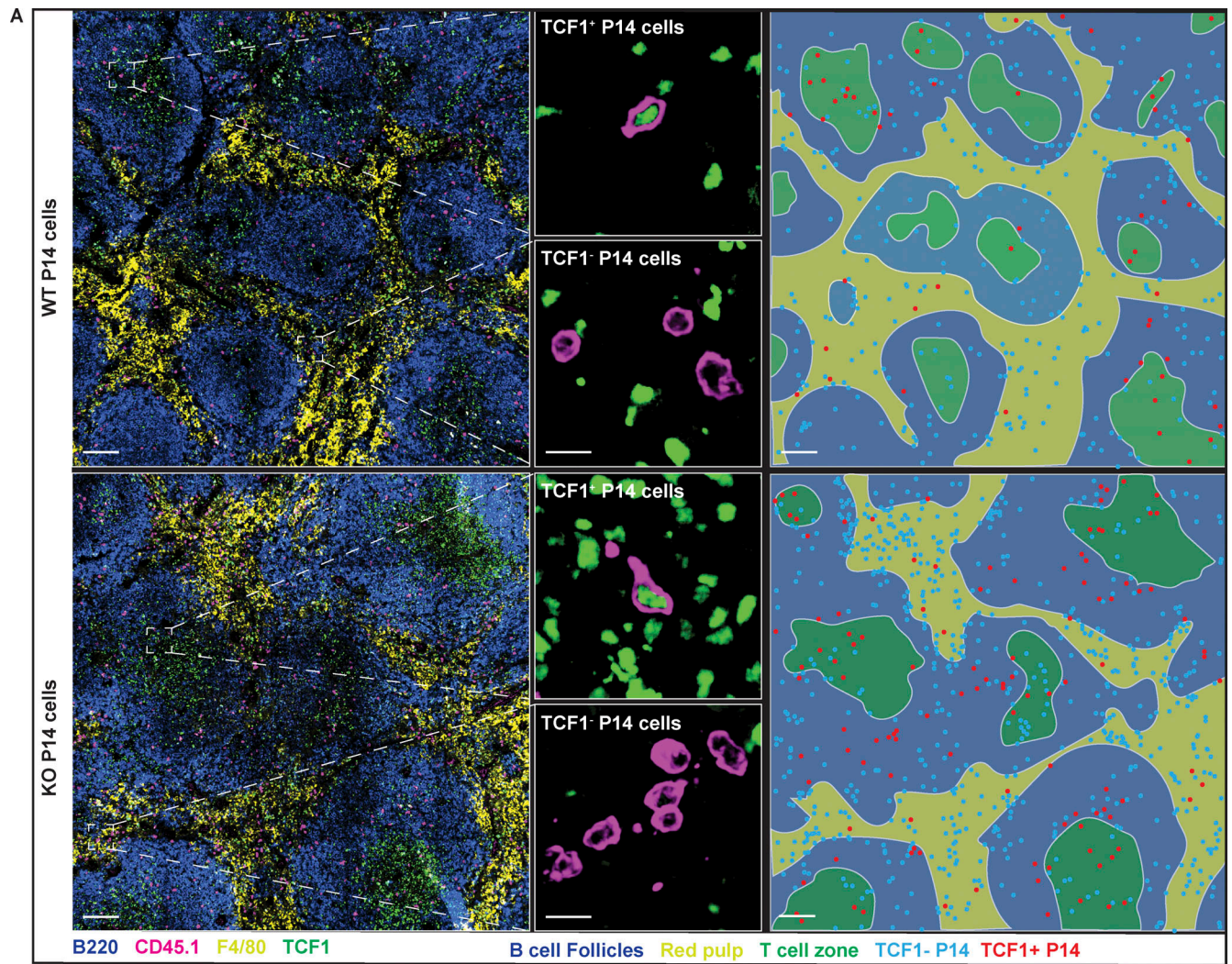
Figure S4. **TGF-β regulates the anatomic location of antigen-specific CD8 T cells activated in chronically infected mice. (A)** CD45.1 WT or KO P14 cells were transferred separately into chronically infected CD45.2 recipient mice (>D45 p.i.). Representative confocal microscopy images of WT and KO P14 cells in the spleen on D20 after transfer. **(B)** Histocytometry analysis showing the distribution of total WT and KO P14 cells in different compartments of the spleen. **(C)** Histocytometry analysis showing the distribution of TCF-1⁻ (left) and TCF-1⁺ (right) WT and KO P14 cells in different compartments of the spleen. The experiment was done with three mice per group. Two regions of 1.25 × 1.25 mm were analyzed per spleen, and the plots show the average. Student's t test; *, $P < 0.05$.
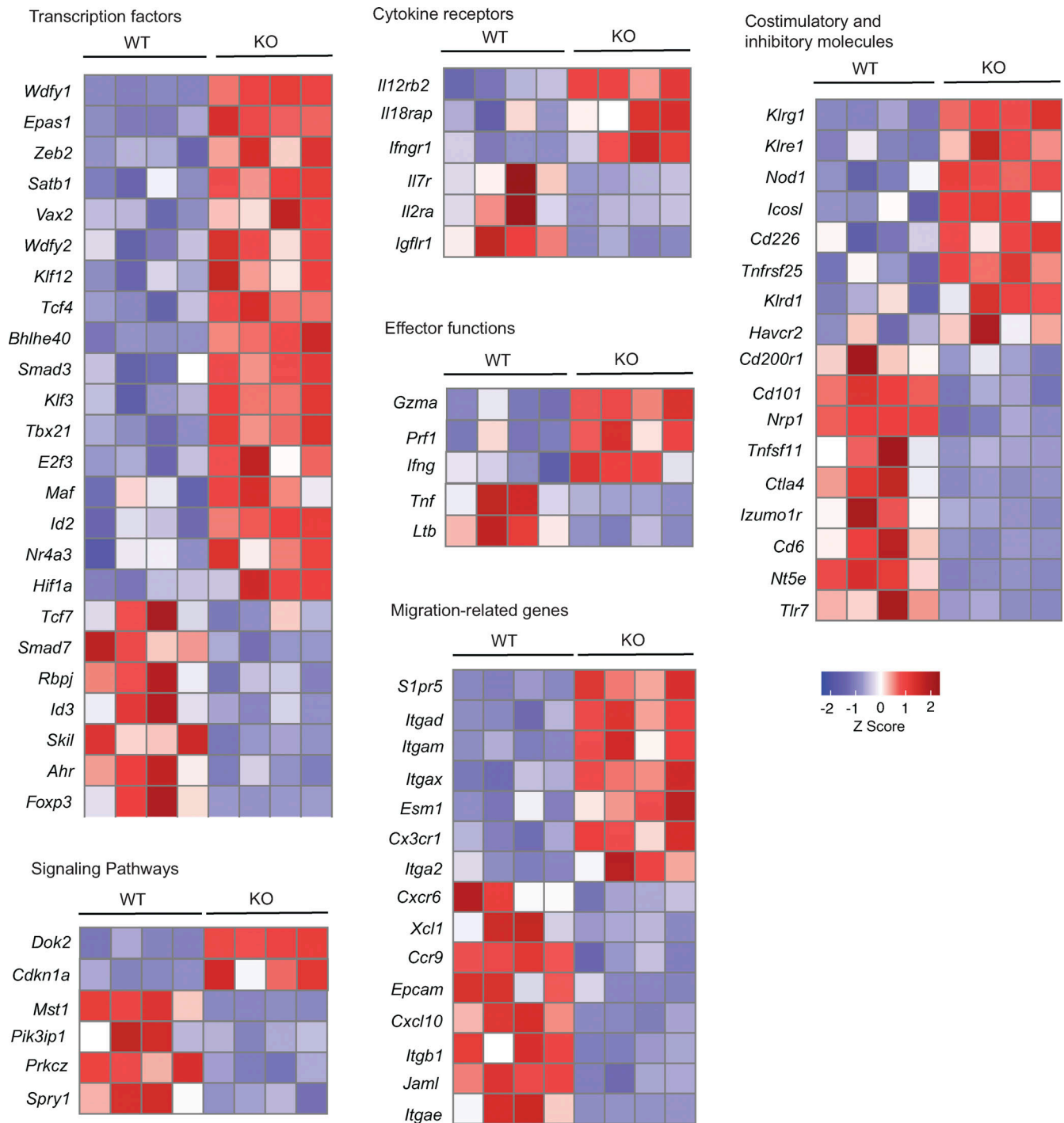
Figure S5. **Selected genes altered by TGF-β receptor deletion in antigen-specific CD8 T cells activated during an established chronic infection.** Heatmap showing the relative expression (z-scores derived from normalized expression values) of selected genes in KO vs. WT P14 cells harvested on D12 after transfer into chronically infected mice. RNA-seq datasets were generated from four biological replicates.

Provided online are Table S1 and Table S2. Table S1 lists genes significantly differentially expressed in D15 and D30 Tim3+ WT vs. KO P14 cells, and in D8, D15, and D30 CXCR5+ WT vs. KO P14 cells (normalized count of 50 or greater in either WT or KO cells; $\log_2$ fold change >0.6 or <−0.6; and adjusted P value <0.05). Table S2 lists genes significantly differentially expressed in WT vs. KO P14 cells 12 d after transfer into chronically infected mice.

Hu et al.
TGF-β regulates CTLs during chronic infection

Journal of Experimental Medicine   S6
https://doi.org/10.1084/jem.20211574